Ore Geology Reviews 61 (2014) 107–119

Contents lists available at ScienceDirect

Ore Geology Reviews

journal homepage: www.elsevier.com/locate/oregeorev

U–Pb dating of hydrothermal zircon from the Dongping gold deposit in North China: Constraints on the mineralization processes

Zhiwei Bao *, Weidong Sun, Chuangjiu Li, Zhenhua Zhao

CAS Key Laboratory for Mineralogy and Metallogeny, Guangzhou Institute of Geochemistry, Chinese Academy of Sciences, 511 Kehua Street, Guangzhou 510640, China

ARTICLE INFO

Article history:
Received 21 October 2013
Received in revised form 11 February 2014
Accepted 12 February 2014
Available online 19 February 2014

Keywords:
Gold deposit
Syenite
Hydrothermal zircon
SIMS
LA–ICPMS
Superimposition
Dongping

ABSTRACT

The Dongping gold deposit is a large deposit with total gold reserves of >100 tons. It is located at the northern margin of the North China Craton, northwestern Hebei province, China. The ore-bodies are hosted by the Devonian Shuiquangou syenite complex and consist mainly of auriferous quartz veins and disseminated ore in the altered and silicified syenite. U–Pb dating of zircon from hornblende syenite on the western margin of the complex yields a crystallization age of 400 ± 3.5 Ma (MSWD = 0.018). Morphology, cathodoluminescence imaging and geochemical classifications of zircon from the first stage of disseminated ore and gray auriferous quartz veins, and from later stage, low grade quartz veins point to their newly crystallized hydrothermal origin. The hydrothermal zircon from the disseminated ore and auriferous gray quartz vein are dated at 389 ± 1.0 Ma and 385 ± 5.7 Ma, respectively, which are detectably younger than but close to the crystallization age of the syenite complex and might have been formed by post-magmatic hydrothermal processes. Both types of ore are dominant in the ore deposit, and we propose that the pervasive, post-magmatic hydrothermal alteration is the main ore forming stage. Hydrothermal zircon from a low grade auriferous quartz vein yields a U–Pb age of ~140 Ma, interpreted as forming during a younger period of superimposed Yanshanian hydrothermal mineralization. Thus, the ore of the Dongping gold mine represents a post-magmatic Devonian hydrothermal ore deposit with Jurassic–Cretaceous hydrothermal overprinting.

1. Introduction

The Dongping gold deposit, which is located in northwestern Hebei province, China, is a large deposit with proven gold reserves of >100 tons. The deposit is hosted in the Devonian Shuiquangou syenite complex. Ore types consist mainly of auriferous quartz veins and disseminated ores (K-feldspar altered and silicified syenite), both of which are characterized by low sulfide and As contents, and a Te-enrichment. The geological and geochemical features of the Dongping gold deposit have been extensively investigated and debated during the past two decades (Bao and Zhao, 2006; Bao et al., 2003; Cook et al., 2009; Fan et al., 2001; Lu et al., 1993, 1997; Mao and Li, 2001; Mao et al., 2003; Mo, 1996; Nie, 1998; Song and Zhao, 1996; Zhang, 1996). Based on ^{40}Ar–^{39}Ar ages of the hornblende from the syenite (327 ± 9 Ma) and hydrothermal K-feldspar from ores (157–177 Ma), Song and Zhao (1996) proposed a model suggesting that the ore metals were leached from the syenite by hydrothermal fluids during Yanshanian (Jurassic–Cretaceous) tectonism. Similarly, based on the ore metal association, close spatial relation with the syenite complex, and S, Si, and Pb isotope compositions of the ore-related minerals, some researchers suggested that the ore deposit is genetically directly related to the syenite complex (Nie, 1998; Nie et al., 2004; Zhang et al., 2005). However, this hypothesis is inconsistent with the more than 200 m.y. gap between the available ages of the syenite complex and ore formation. Moreover, some other workers argued that the low salinity, CO_2-rich ore fluids reflect a metamorphic hydrothermal origin (Hart et al., 2002; Mao et al., 2003), which is typical of most orogenic gold deposits (e.g., Goldfarb et al., 2001). Orogenic gold deposits are usually associated with greenschist phase metamorphic rocks (e.g., Goldfarb et al., 2001), which is likely due to the pyrite to pyrrhotite transition during prograde metamorphism from greenschist to amphibolite phases (e.g., Sun et al., 2013). The Dongping gold deposit, however, is located in the central part of the Shuiquangou syenite, which is not the usual geologic setting for orogenic gold deposits. More importantly the reported argon ages of ore formation are inconsistent with those of the regional tectonic and magmatic events (Hu and Song, 2002, 2003; Li and Bao, 2012; Miao et al., 2002). The suspect ^{40}Ar–^{39}Ar ages for the magmatic hornblende and hydrothermal K-feldspar might be the result of partial resetting by later thermal events or excess ^{40}Ar inherited from the feldspars during K-feldspathization. The mixing of two generations of K-feldspar has also been proposed as a possible explanation of the spurious ages (Berger, 1975; Kuiper, 2002). Obviously, the geochemical and metallogenetic understanding of the Dongping gold deposit is hindered by a lack of precise dating of the ore forming process.

* Corresponding author. Tel.: +86 20 8529 0105.
E-mail address: baozw@gig.ac.cn (Z. Bao).

http://dx.doi.org/10.1016/j.oregeorev.2014.02.006
0169-1368/

Studies have demonstrated that precise U–Pb dating of hydrothermal zircon from altered rocks and quartz veins of ore deposits is a good tool for dating hydrothermal ore formation (Claoué Long et al., 1990; Kerrich and King, 1993; Pelleter et al., 2007; Toscano et al., 2014; Zartman and Smith, 2009). However, presumed hydrothermal zircon in altered rocks and ores might alternately be hydrothermally altered wall rock zircon, or zircon mechanically entrapped from the wall rocks. Therefore, U–Pb dating of zircon must be accompanied by detailed mineralogical and chemical study to indentify its source. Hydrothermal zircon, either directly precipitated from fluid solution or formed from hydrothermal alteration of country rock, often shows cathodoluminescence images and rare earth element compositions different from that of magmatic zircon (Hoskin, 2005; Pelleter et al., 2007; Yang et al., 2013).

In order to precisely date the ore-forming processes, LA–ICPMS and SIMS zircon U–Pb dating, CL imaging, and LA–ICPMS trace element analysis were carried out on hydrothermal zircon from auriferous quartz veins and K-feldspar altered disseminated ores obtained from the Dongping gold deposit, and magmatic zircon from hornblende syenite of the Shuiquangou syenite complex. A metallogenetic model for the Dongping gold deposit is proposed based mainly on the new dating results.

2. Geological background

The Dongping gold deposit is situated in Chongli county, Hebei province. Tectonically, it is located on the western end of the Yanshan orogen at the northern margin of the North China Craton, about 10 km to the south of the Shangyi–Chongli–Chicheng fault (Fig. 1). The Shangyi–Chongli–Chicheng fault belt, a deep-rooted fault that extends along the southern boundary of the Inner Mongolia axis on the edge of the craton, was formed in the Mesoproterozoic, and was subsequently reactivated in the Neoproterozoic, Paleozoic, and Mesozoic (Hu et al., 2003; Zhang et al., 2007). The fault system is a ductile to brittle, multi-stage thrust fault, and it is still an important seismically active zone (Ma and Zhao, 1999).

Archean and Paleoproterozoic metamorphic rocks are widespread in the region. The Sanggan metamorphic complex, consisting of Archean amphibolite and granulite generated from a series of mafic to felsic volcanic rocks and clastic sediments, is widespread to the south of the Shangyi–Chongli–Chicheng fault. The Paleoproterozoic Hongqiyingzi Group, consisting of marble, quartzite, amphibolites, and gneiss generated from a series of marine volcanic and sedimentary rocks, occurs to the north of the fault. Mesoproterozoic marine sedimentary rocks occur sparsely in the southeastern corner of the deposit area. Early Cretaceous Zhangjiakou Group continental volcanic–sedimentary rocks occur in the southern and southeastern part of the mining area.

The Devonian Shuiquangou syenite complex intruded Archaean metamorphic rocks and are locally unconformably overlain by Early Cretaceous volcanic rocks. The syenite complex is NW-trending and dips to the south, with an outcropping area of about 350 km^2. The syenite complex is composed of augite–hornblende–alkali feldspar syenite, alkali feldspar syenite, quartz–alkali feldspar syenite, and quartz syenite. It is noteworthy that the lithology of the complex changes

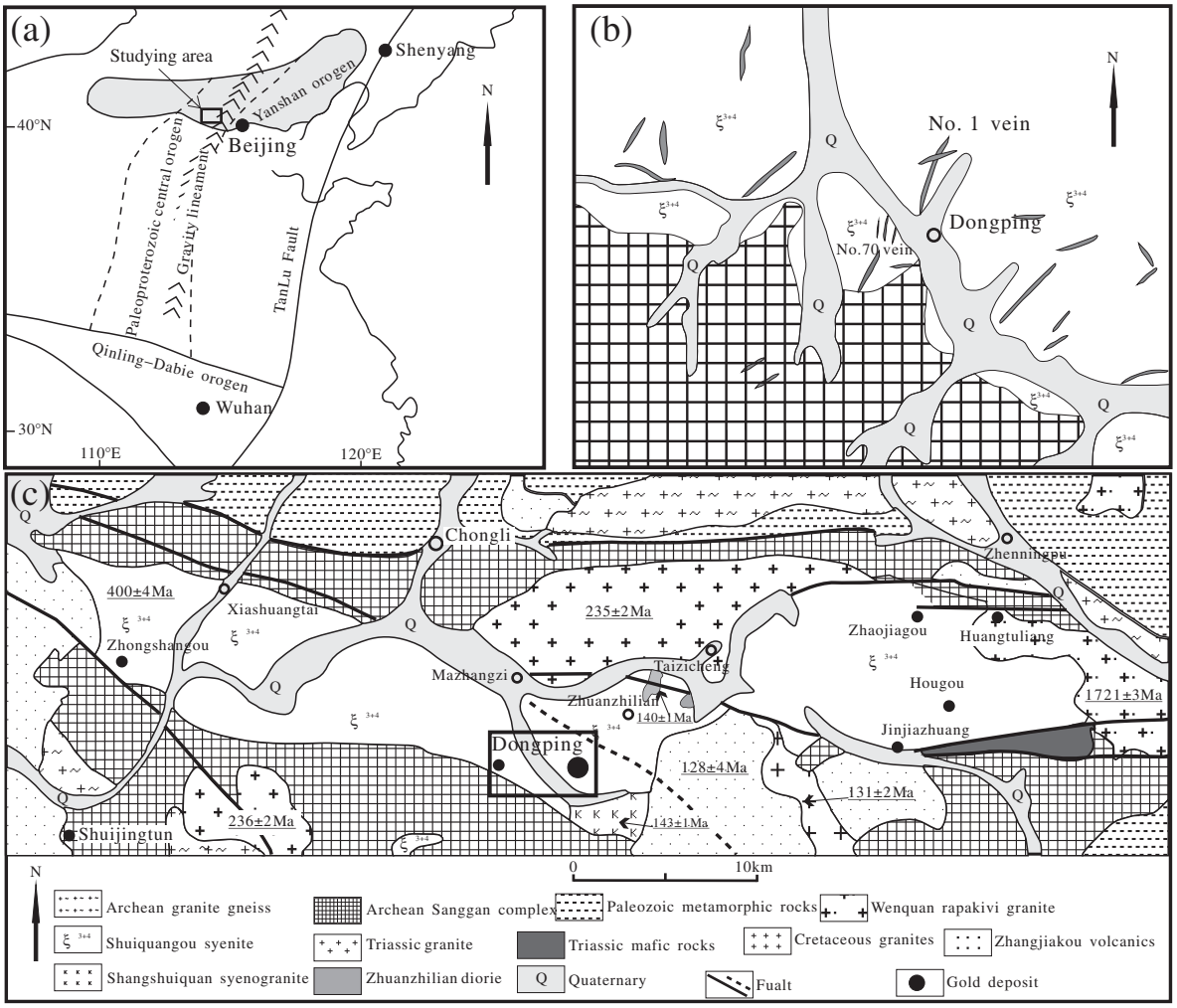

Fig. 1. Geological sketch map of the Shuiquangou syenite complex and distribution of the related gold deposits in Northwest Hebei province.

gradually without any distinguishable boundary. The contents of CaO, MgO, FeO, and Fe_2O_3 decrease, whereas K_2O, Na_2O, and SiO_2 increase eastwards as the rock types change from augite–hornblende–alkali feldspar syenite to quartz syenite. Geochemical and isotopic characteristics of the syenites show that they were mainly derived from partial melting of the upper mantle (Bao et al., 2003; Jiang, 2005). Intensive post-magmatic hydrothermal alteration of the syenite was observed at the mining area, which includes silicification and K-feldspathization during which euhedral allanite was replaced by anhedral allanite, and chervkinite-(Ce) was replaced by an allanite and ilmenite association, which is likely the cause of the REE tetrad in altered rocks. The inferred composition of the hydrothermal fluids is characterized by high alkalic and F contents (Jiang, 2006, 2003). Several gold deposits including the Dongping, Zhongshangou and Huogou deposits have been exploited in the inner contacts or inside of the Shuiquangou syenite complex.

SHRIMP zircon U–Pb dating of the syenites from a location adjacent to the Dongping mining area and from the eastern part of the complex yield ages of 390 ± 6 Ma and 386 ± 7 Ma, respectively (Miao et al., 2002). In addition to the Shuiquangou syenite complex, which is the host for the Dongping and several other gold deposits, there are a few Mesozoic intrusions adjacent to the syenite. The Triassic Honghualiang biotite syenogranite and Guzuizi coarse-pegmatitic porphyritic syenogranite have SHRIMP zircon U–Pb ages of 235 ± 2 Ma and 236 ± 2 Ma, respectively, and occur to the north and south of the syenite (Jiang et al., 2007; Miao et al., 2002). Both Triassic granites are adakitic and might be derived from partial melting of the lower crust during the closure of the Paleo-Asian Ocean in the Late Permian (Jiang et al., 2007). Cretaceous magmatism is widespread in the region, including the Zhuanzhilian diorite (139.5 ± 0.9 Ma, SHRIMP zircon U–Pb, Jiang et al., 2007), Shangshuiquan syenogranite (142.5 ± 1.3 Ma, SHRIMP zircon U–Pb, Miao et al., 2002), and Beizhazi monzogranite (130.5 ± 1.5 Ma, SHRIMP zircon U–Pb, Li and Bao, 2012). The Cretaceous granitic rocks likely formed in extensional tectonic settings related to Mesozoic lithospheric thinning of the North China Craton (e.g., Deng et al., 2007; Gao et al., 2002; Li et al., 2013; Liu et al., 2012; Menzies et al., 2007; Wilde et al., 2003; Xu et al., 2013; Zhu et al., 2012).

Faulting in the study area is well-developed. In addition to the first-order east-west trending Shangyi–Chongli–Chicheng fault, which extends down to the Moho (Hu and Song, 2002), there are several subordinate faults, particularly the Zhongshangou–Honghuabei–Shangshuiquan fault, which controlled the emplacement of the syenites and might also have been the main conduit for the hydrothermal gold activity. Orebodies are hosted in NNE- and NW-trending, third-order brittle–ductile fractures (Song and Zhao, 1996).

The Dongping gold deposit is located in the central part of the Shuiquangou syenite near the village of Dongping, where the ore bodies occur in the southern contact zone of the syenite. The deposit is hosted in a series of NNE-striking subparallel, commonly en echelon auriferous quartz vein swarms and quartz-K-feldspar veinlets within syenite. All together 69 auriferous veins have been delineated in the mining area across a surface area of more than 21 km^2. The veins are enveloped by intensively K-feldspathized syenite, ranging commonly from a few tens of cm up to a few m thick, and even up to 30 m at depths in the mine. The ore vein No.1–70 consists of more than 60 orebodies, containing 80% of the total gold resources. This ore vein is more than 1300 m long with width varying from tens of m to more than 500 m, controlled depth extending to more than 800 m (Fig. 2). Individual orebodies are generally 200 to 400 m long, 0.12 to 36 m thick and extend downwards for 100 to 600 m, which are commonly striking 20–30° NE and NW dipping with angel of inclination around 30–50°. The ore grade averages 6 g/t Au throughout the mine, but the grade for individual orebody varies between 4 and 23 g/t. Gold is generally fine-grained and rarely visible in hand specimen. The ore types vary from surface downwards, with auriferous quartz vein in the upper part of the orebodies, quartz stockworks and disseminated ores in the middle, and disseminated ores in the lower part. The ores are low in sulfides (<3%), with major

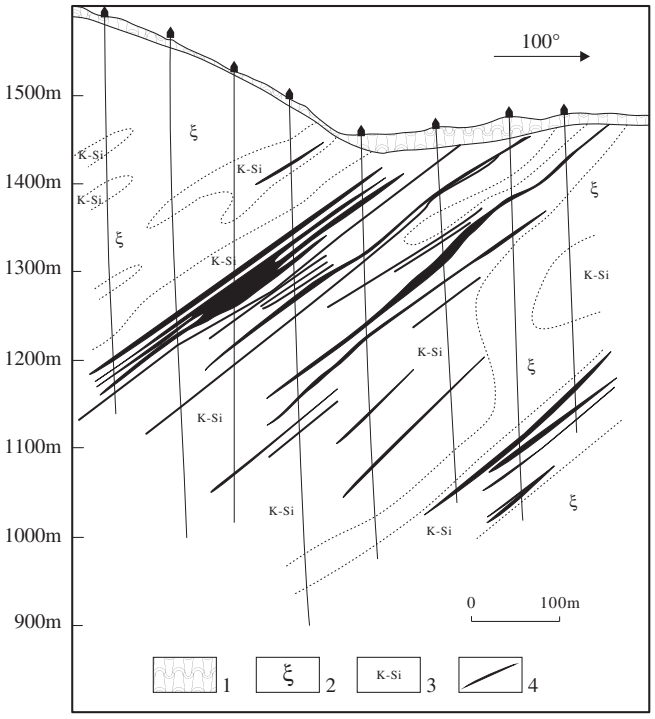

Fig. 2. Cross section of the Dongping gold deposit. 1. Quaternary; 2. Syenite; 3. K-feldspathized and silicified syenite; 4. Quartz vein.

sulfides consisting of pyrite, with minor chalcopyrite, galena, and sphalerite, and lesser amounts of the oxides, specularitic hematite, and magnetite. Gangue minerals include quartz, microcline, and albite. Gold mainly occurs as native gold, calaverite, electrum, and petzite. The Te/Au ratio of the ores has an average value of 0.71 but is observed to increase with the grade of Au (Zhang et al., 2001). Wall rock alteration includes extensive silicification with formation of K-feldspar, albite, pyrite, sericite, chlorite, and epidote. Fluid inclusion results show that the ore-forming fluid was moderately saline (5%–7% NaCl), ranging in temperature from mesothermal to hypothermal (homogenization temperatures of 250 °C–380 °C), and chemically of the NaCl–CO_2–H_2O type (Fan et al., 2001; Mao et al., 2003). Ore forming processes can be divided into three stages from early to late, including: (1) gold-bearing quartz-K-feldspar veins and stockworks along with enveloping disseminated sulfide and gold zones (Fig. 3a,b), (2) gold-bearing quartz veins and auriferous quartz-polymetallic sulfide veins (occurring locally as veinlets in the earlier stage of auriferous quartz veins) (Fig. 3c), and (3) barren calcite-quartz veins (rare visible in the field, commonly occur as fine veinlet under microscopy). Gold mineralization mainly took place in the first stage while the second stage represents latter hydrothermal superimposition. However, cross-cutting quartz veins and overprinting by later K-feldspar and quartz are common (Fig. 3d).

3. Sampling and analytical methods

Investigations on the behavior of zircon, apatite and other accessory minerals during hydrothermal alteration and the Tetrad REE effect of the Shuiquangou syenite show that the zircon in the mining area is heavily damaged (Zhao et al., 2010). Because the syenites in the mining area underwent intense alteration and the SHRIMP ages by Miao et al. (2002) lack internal structural information, it was deemed desirable to redate the syenite. To minimum the possibility of hydrothermal overprinting of the U–Pb isotope system and, thus, to justify the reliability of the isotopic dating, pristine zircon from unaltered hornblende-alkali feldspar syenite situated about 20 km away from the mining area in the western part of the syenite complex, were also analyzed using the LA–ICPMS method.

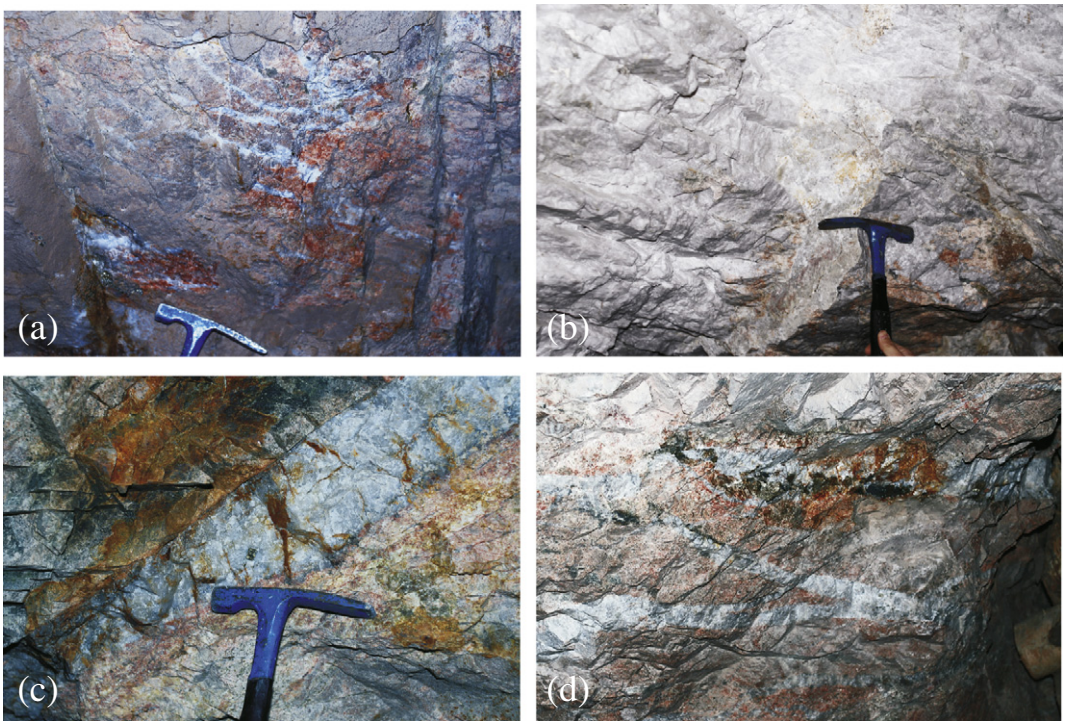

Fig. 3. Photographs from underground exposures in the Dongping gold deposit. (a) Altered syenite with quartz veinlets crosscut by later stage quartz-sulfide veins; (b) broad gray quartz vein; (c) low grade quartz vein; (d) low grade quartz veins with localized sulfides enrichment.

The hornblende syenite sample (D-06) was collected from west side of the syenite complex, and it is gray to pinkish consisting of microcline, albite, diopside, aegirine augite, ferropargasite, achromaite, and accessory minerals including zircon, sphene, and rutile. Three ore samples, representatives of three different ore-types, were collected from the Dongping deposit. Sample BDP-4 is from auriferous disseminated and stockwork mineralization in the syenite collected at the 1200 m level of the No. 1-70 orebody. The rock is pinkish due to intense K-feldspar formation. Sample D-77 was collected from a 30-cm-wide, gray auriferous quartz vein with abundant sulfides and grading about 200 g/t Au at the 1224 m level of the No. 1-70 vein. Sample D-19 was collected from a 10-cm-wide, low-grade, milky white auriferous quartz vein at the 1184 m level of the No. 1-70 vein system. No. 1-70 at 1184 m level from a 10-cm-wide, low-grade, milky white auriferous quartz vein. The quartz vein is surrounded by a moderate amount of K-feldspar alteration; smaller sulfide-bearing quartz veins commonly cut across or run subparallel to the big quartz vein.

Zircon was separated using conventional crushing, heavy liquid, and magnetic separation techniques and hand-picked under a binocular microscope. It was then mounted onto epoxy resin disks and polished to near half thickness in order to expose internal structures. Fracture- and enclave-free grains and/or spots within grains were selected based on microscopy observation and cathodoluminescence images for analyses.

Uranium–Pb dating of zircon from the disseminated ore and unaltered hornblende syenite, and in-situ trace element analyses of all zircon grains were performed using an Agilent 7500a ICP-MS coupled with a Resonetics RESolution M-50 (193 nm ArF excimer) laser system at the State Key Laboratory of Geochronology and Geochemistry, Chinese Academy of Sciences. Sample mounts were placed in a specially-designed double volume sample cell flushed with Ar and He. Laser ablation was operated at a constant energy (81 mJ cm^{-3}) at a repetition rate of 10 Hz and a spot diameter of 31 μm. The ablated material was carried by He–Ar gas via a Squid system to homogenize the signal to the ICP-MS (Li et al., 2012a; Liang et al., 2009). Off-line selection and integration of background and analyzed signals, and time-drift correction and quantitative calibration for trace element analyses and U–Pb dating were performed by an in-house program ICPMSDataCal (Liu et al., 2010). External standard glass NIST SRM 610 and standard zircon Tomora were used for external calibration (Black et al., 2003; Li et al., 2012a). ^{29}Si was used as the internal standard. Common Pb correction and ages of the samples were calculated by using ComPbCorr#3_17 (Andersen, 2002). Concordia diagrams and weighted mean calculations were made using Isoplot/Ex_ver3 (Ludwing, 2003). Uncertainties are listed in Table 1 and the weighted mean ages are quoted at the 95% confidence level. The analytical method and data treatment are similar to those of Yuan et al. (2004) and Liang et al. (2009).

Measurements on zircon grains from the two quartz veins were conducted using the CAMECA ims-1280 SIMS at the Institute of Geology and Geophysics, Chinese Academy of Sciences in Beijing, mainly because the zircon grains from the quartz veins are too small to analyze using LA-ICPMS method. Details of the procedures and data handling are the same as described by Li et al. (2009). Uncertainties for individual analyses in the data table are reported at a 1σ level; mean ages are quoted at the 95% confidence interval by pooling multiple U/Pb and Pb/Pb analyses for the same samples. Data reduction was carried out using the Isoplot/Ex v.3.0 program (Ludwig, 2001).

4. Results

4.1. Cathodoluminescence imaging

Pristine zircon grains from the hornblende syenite (sample D-06) are stubby prisms, colorless to light yellowish. Cathodoluminescence (CL) images of most zircon grains show oscillatory zoning, indicating a magmatic origin (Fig. 4a).

Zircon grains from the disseminations in the altered syenite (BDP-04) are coarse, yellowish to brown, irregular grains or aggregates, and exhibit textureless or mosaic textures, weak cathodoluminescence; relicts of magmatic oscillatory zoning are rare (Fig. 4b).

Zircon grains from the gray auriferous quartz vein (D-77) are brownish and composed of two groups. One group of zircon grains shows core-overgrowth structures on CL images, which suggests

Table 1
REE concentrations of zircons from the ores and hornblende syenite (ppm).

	La	Ce	Pr	Nd	Sm	Eu	Gd	Tb	Dy	Ho	Er	Tm	Yb	Lu	δCe	$(Sm/La)_N$	REE
Zircons from the hornblende syenite																	
D06-01.02	0.04	13.4	0.03	0.33	0.46	0.34	3.42	1.05	13.1	6.12	33.1	8.7	110	27.5	175	49.4	217
D06-01.03	0.04	19.1	0.1	2.06	2.36	1.19	9.77	3.32	38.1	15.9	82.2	20.9	245	58.9	82.0	121	499
D06-01.04	0.05	17.9	0.08	1.04	1.53	0.86	7.55	2.58	30.4	13.2	69.0	17.7	205	50.0	66.6	43.2	417
D06-01.05	0.05	7.84	0.04	0.34	0.49	0.4	3.27	1.02	13.1	5.79	31.3	8.5	106	26.7	87.1	31.7	205
D06-01.06	0.06	16.4	0.12	1.52	2.07	1.2	9.8	3.07	35	15.1	80.3	20.5	247	61.5	67.3	115	493
D06-01.07	0.05	8.67	0.04	0.48	1.13	0.52	4.46	1.38	17.3	7.35	40.2	10.4	121	29.8	86.8	77.00	243
D06-01.08	0.04	16.3	0.06	1.02	1.84	0.88	9.43	3.09	38.9	16.7	87.4	21.4	246	57.1	117	162	500
D06-01.09	0.17	18.4	0.08	0.98	1.72	1.01	8.5	3.01	39.7	18.4	101	25.6	296	71.9	17.7	4.51	586
D06-02.01	0.05	10.6	0.03	0.47	0.78	0.59	5.14	1.74	21.6	10.3	57.5	14.9	182	45.9	72.3	26.30	352
D06-02.02	0.51	15.7	0.2	0.96	1.14	0.42	3.96	1.42	19.1	8.56	49.5	13.1	164	41.4	12.1	3.48	320
D06-02.03	0.04	10.5	0.12	1.88	2.1	1.27	9.58	3.1	35.9	14.8	77.7	18.8	215	51.2	37.4	83.4	442
D06-02.04	0.04	13.2	0.04	0.69	1.24	0.73	5.89	2	27.1	12.6	70.7	18.3	221	55.0	81.0	53.4	429
D06-02.05	0.04	7.45	0.04	0.27	0.69	0.33	2.98	1.06	13.3	5.85	32.5	8.76	109	27.7	43.5	24.3	210
D06-02.06	0.04	8.91	0.03	0.3	0.59	0.3	2.75	0.91	12.2	5.37	29.2	7.79	96.1	24.2	60.1	20.8	189
D06-02.07	0.03	12.5	0.05	0.27	0.53	0.32	3	1	13.9	7	41.3	11.3	149	40.3	87.8	30.4	280
D06-02.08	0.06	9.25	0.03	0.47	1.12	0.49	5.32	1.86	21.6	9.23	43.6	10.3	116	26.1	54.1	31.5	245
D06-02.09	0.03	9.6	0.04	0.42	0.74	0.45	3.78	1.12	14.2	6.89	38.8	10.5	135	36.7	75.5	42.5	258
Zircons from the auriferous milky quartz vein																	
D-19.1	0.18	44	0.13	1.44	3.6	1.73	23.7	7.86	93.8	39.3	181	42.7	432	85.3	70.8	31	957
D-19.2	0.34	77.4	0.8	8.75	10.5	6.71	44.4	12.1	115	41	176	40	421	84.9	36.4	47.6	1039
D-19.19	0.74	35.7	0.79	5.46	5.22	2.37	19.7	6.53	75.5	28.2	135	30.9	324	65.9	11.5	10.9	735
D-19.24	1.71	84.6	1.5	10.1	8.96	2.91	32.2	9.82	101	37.1	161	35.5	357	71.6	13	8.12	915
D-19.3	0.11	3.22	0.11	1.13	1.51	0.24	7.88	3.38	43	18	90	21.4	232	46.3	7.08	20.5	468
D-19.20	5.58	61.5	4.36	28	19.6	2.35	54.5	16.5	175	63.9	281	61.3	602	112	3.06	5.42	1487
D-19.21	0.21	27.9	0.38	5.05	8.98	1.14	33.6	10.6	103	33.7	138	28.9	269	46.3	24.2	66.2	707
D-19.23	4.02	17.9	3.01	23.2	18.5	2	64.5	21.3	229	88.8	400	86.6	860	164	1.26	7.12	1982
D-19.25	0.17	6.41	0.12	1.88	3.26	0.45	21.5	8.34	104	41.6	186	42.1	417	77	11.1	29.2	909
D-19.26	0.18	5.75	0.15	1.75	3.69	0.41	21.3	8.06	99.5	39.4	179	39.6	394	72.2	8.47	30.7	866
D-19.27	0.17	6.45	0.1	0.96	3.13	0.32	15.6	6.32	85.7	33.8	161	34.5	354	68.3	12.8	29	771
D-19.28	10.4	40.7	4.27	23.8	11.6	1.74	34.2	11	121	45.3	218	49.4	510	103	1.5	1.71	1184
Zircons from the auriferous gray quartz vein																	
D-77.8	0.15	10.6	0.12	1.83	1.99	0.82	6.27	1.7	21.2	9.5	52.8	14.9	192	50.3	19.5	20.3	364
D-77.12	0.1	46.4	0.11	1.42	4.09	1.68	20.7	7.08	87.5	39.2	212	57.4	728	175	109	64.6	1381
D-77.16	0.24	18.3	0.08	0.74	0.89	1.19	4.84	1.67	21.9	8.82	48.9	12.7	169	49.6	32	5.87	339
D-77.18	0.68	16.8	0.26	1.76	1.29	0.68	9.47	3.7	50.6	20.6	104	24.3	260	50.3	9.78	2.94	544
D-77.10	86.7	473	77.6	453	147	128	150	24.5	190	58	250	56.3	559	101	1.41	2.62	2753
D-77.11	0.18	34.8	0.13	1.59	2.52	0.23	8.93	2.22	19.4	6.16	22.7	4.74	45.8	9.59	55.5	21.2	159
D-77.17	0.14	22.1	0.1	1.16	2.13	0.26	8.04	2.28	27.9	10.1	45.2	10	101	19	44.7	23.2	249

entrained from the metamorphic country rocks. Indeed, enclaves of metamorphic rock are commonly observed near the sampling site in the adit. The other group shows rather obscure zoning or no internal texture on CL images (Fig. 4c).

Zircon grains from the milky white auriferous quartz veins (D-19) are yellow to brownish, transparent to translucent, and elongated to stubby prisms (<100 μm). These zircon grains show ambiguous or no oscillatory zoning on CL images (Fig. 4d).

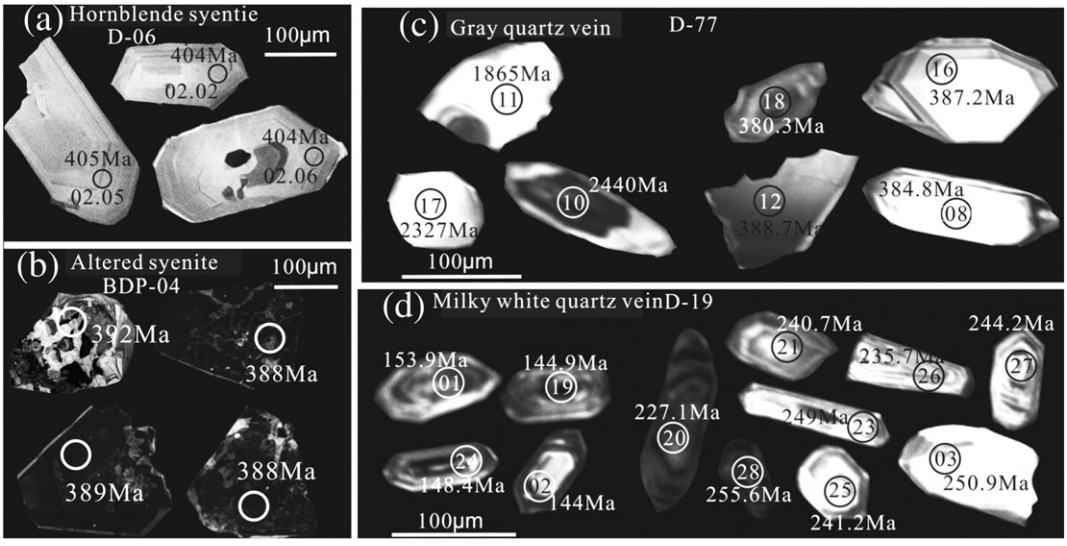

Fig. 4. Cathodoluminescence images of zircons from the syenite and ores of the Dongping gold deposit.

Zircon grains from both the disseminated and quartz vein ores show CL images similar to the internal structures of reported hydrothermal zircon (Lawrie et al., 2007; Pettke et al., 2005; Wu and Zheng, 2004).

4.2. REE concentration

The REE concentrations of the pristine zircon grains from the hornblende syenite are low ($\sum$REE = 189–586 ppm), with normalized patterns characterized by a steeply-rising slope from the LREE to the HREE and with pronounced positive Ce anomalies (with δCe values mostly higher than 50) and insignificant negative Eu anomalies (δEu = 0.60–0.97) (Table 1, Fig. 5a), which are typical for magmatic zircon (Hoskin and Schaltegger, 2003). In contrast to pristine zircon, zircon grains from the disseminated ore are enriched in REE ($\sum$REE = 510–9933 ppm), exhibiting flat or less steep REE patterns with less significant Ce anomalies (δCe = 1.83–5.05) and positive Eu anomalies (δEu = 0.96–1.27) (Fig. 2, Zhao et al., 2010).

The REE concentrations of the hydrothermal zircon grains from the gray auriferous quartz vein vary between 339 and 1381 ppm, showing LREE depleted chondrite normalized REE patterns. However, the LREEs are relatively more enriched than those of the pristine zircon grains and have variable Ce and Eu anomalies (δCe = 9.8–109, δEu = 0.56–1.75, Fig. 5b). The REE concentrations of the zircon grains entrained from the metamorphic wall rocks were not analyzed in this study.

The REE concentrations of zircon grains from the milky white auriferous quartz vein (D-19) vary between 707 and 1982 ppm, and are significantly higher than those of the pristine zircon. These zircon grains can be roughly divided into two groups according to Ce and Eu anomalies. The first group consists of four grains (analysis Nos. 01, 02, 19, and 24), exhibiting ambiguous zoning on CL images, pronounced Ce anomalies (δCe = 11.5–70.5) and weak negative Eu anomalies (δEu = 0.52–0.95, Fig. 5c). The other group (determination Nos. 0, 20, 21, 2, 25, 26, 27, 28), with ambiguous zoning or no clear internal textures on CL images, shows less pronounced Ce anomalies (δCe = 1.26–24.2) and significant negative Eu anomalies (δEu = 0.14–0.26, Fig. 5d).

On a discrimination diagram of $(Sm/La)_N$–La (ppm) for zircon, almost all of the zircon grains from the hornblende syenite plot in the magmatic field. In contrast, almost all of the zircon grains from the auriferous quartz veins and disseminated ores (except the interpreted metamorphic zircon grains) are scattered and trend away from the magmatic zircon field. These zircon grains plot in the neocrystallized hydrothermal zircon area of the diagram (Fig. 6), which indicates that the zircon grains from ores are almost certainly of hydrothermal origin.

4.3. U–Pb results

Thorium and uranium contents of pristine zircon from the hornblende syenite (sample D-06) vary between 20.9–110 ppm and 48.7–209 ppm, respectively, with Th/U ratios of 0.35–0.65, which is typical for magmatic zircon. Seventeen LA–ICPMS U–Pb measurements of pristine zircon yield similar $^{206}Pb/^{238}U$ ages with a weighted average of 400 ± 3.5 Ma, MSWD = 0.018 (Table 2, Fig. 7a). This age is taken to represent the age of crystallization for the hornblende syenite and is slightly but detectably older than previously published SHRIMP data (Miao et al., 2002).

Zircon grains from the disseminated ore (BDP-04) exhibit much more varied Th and U contents and Th/U ratios compared to the magmatic zircon, ranging from 13.1 to 5383 ppm, 94 to 17563 ppm, and 0.08 to 0.92, respectively. These zircon grains commonly have higher contents of Th and U. Considering the morphology, texture, CL images, and Th, U, and REE signatures, we propose that these are hydrothermal zircon; the higher Th, U and REE contents are likely contributed from post-magmatic hydrothermal solutions (Zhao et al., 2010). The 35 LA–ICPMS U–Pb analyses of zircon grains fall into two populations (Table 3, Fig. 7b, c,d). The first cluster of 14 spots yields a weighted average $^{206}Pb/^{238}U$ age of 389 ± 1.0 Ma (MSWD = 0.20). The second cluster of 9 spots yields a weighted mean age of 357.5 ± 3.0 Ma (MSWD = 0.37). As no tectono-magmatic activity was recognized in the region, age of the 9 spots might be the result of partly resetting of the U–Pb isotopic system during later

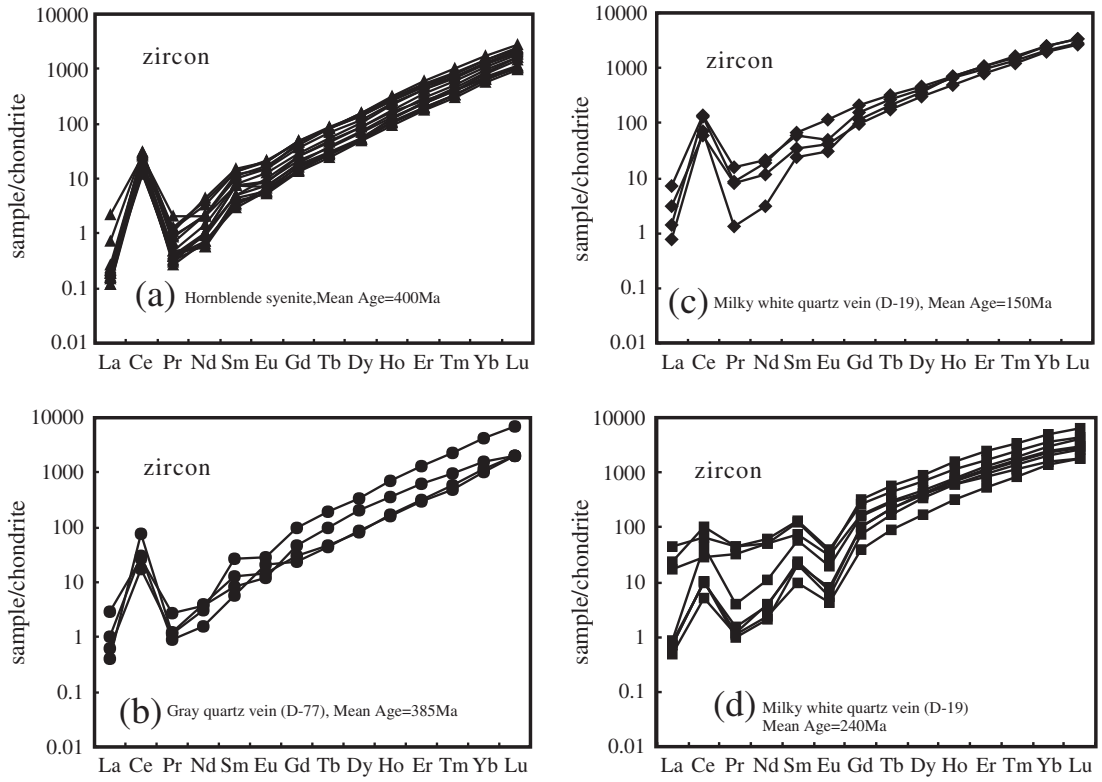

Fig. 5. Chondrite normalized REE patterns of zircons from the hornblende syenite and auriferous quartz veins (chondritic data from Boynton, 1984).

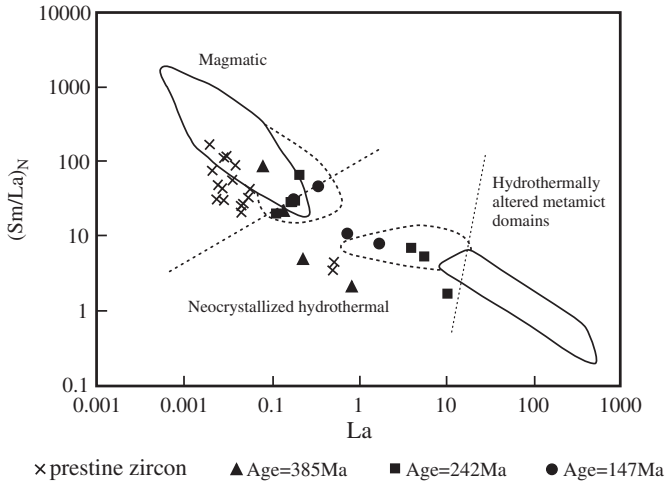

Fig. 6. Discriminant diagram of $(Sm/La)_N$ versus La for zircons from the syenite and auriferous quartz veins (after Hoskin, 2005; Kirkland et al., 2009).

stage hydrothermal alteration and are geologically meaningless (Chen et al., 2011).

The CAMECA ims-1280 SIMS analyses were conducted on zircon grains from both the gray and milky white auriferous quartz veins (Table 4). Three of the 19 analyses (point Nos. D-77.10, D-77.11, and D-77.17) of zircon grains from the auriferous quartz veins yield $^{206}Pb/^{238}U$ apparent ages of 2050 Ma, 1805 Ma, 2284 Ma, respectively. Considering the core-overgrowth CL images, these ages are likely related to the common occurrence of metamorphic rock enclaves in the syenite at the lower part of the No.1-70 orebody. These zircon grains must have been acquired from metamorphic rocks that underwent high grade metamorphism in the Paleoproterozoic. The other 16 analyses can be divided into three groups (Fig. 8a), within which two groups come from the milky white auriferous quartz vein.

Hydrothermal zircon grains from the auriferous gray quartz vein are characterized by low Th and U contents, and low Th/U ratios as well, varying in ranges of 4–28 ppm, 54–521 ppm, and 0.04–0.55, respectively. Four analyses yield a weighted mean $^{206}Pb/^{238}U$ age of 385 ± 5.7 Ma (MSWD = 0.42) (Fig. 8b), which is essentially identical to the LA–ICPMS result of 389 ± 1.0 Ma, close to but resolvably younger than the age of the syenites (400 ± 3.5 Ma).

It is noteworthy that the zircon grains with $^{206}Pb/^{238}U$ age of ~385 Ma from the disseminated ore and quartz auriferous vein have high U and Th contents and low Th/U ratios, similar to the zircon grains from the syenite rocks from the Dongping and Hougou areas analyzed by Miao et al. (2002). These zircons all have identical ages, but are strikingly different from those of the magmatic zircon grains in the western part of the syenite complex (Fig. 9).

Eight analyses of one group of zircon grains from the milky white auriferous quartz vein are relatively low in Th and U contents, and Th/U ratios, varying in ranges of 81–574 ppm, 215–1626 ppm, and 0.22–0.88, respectively. The 8 $^{206}Pb/^{238}U$ ages show some scatter and range from 227 to 256 Ma with a weighted mean age of 242 ± 6.8 Ma (MSWD = 6.3, Fig. 8c), which is roughly contemporaneous with the Triassic granite intrusion in the region (Jiang et al., 2007; Miao et al., 2002). The other group of zircons from the milky white auriferous quartz veins is generally more enriched in Th and U, 320–4566 ppm and 396–1824 ppm, respectively, with high Th/U ratios (Th/U = 0.66–2.50). Four analyses yield a weighted average $^{206}Pb/^{238}U$ age of 147.8 ± 2.3 Ma (MSWD = 3.3, Fig. 8d), which is similar to the U–Pb age of hydrothermal zircon (140.3 ± 1.4 Ma) reported by Li et al. (2010) as well as the age of the Early Cretaceous Shangshuiquan syenogranite adjacent to the deposit (SHRIMP zircon U–Pb, 142.5 ± 1.3 Ma, Miao et al., 2002).

The hydrothermal zircon grains with a $^{206}Pb/^{238}U$ age of 385 ± 5.7 Ma may be interpreted to be formed during a post-magmatic stage of the Shuiquangou syenite emplacement, whereas the hydrothermal zircon grains of 147.8 ± 2.3 Ma may have been precipitated during younger episodes of hydrothermal ore formation.

5. Discussion

5.1. Timing of gold mineralization

Many geochronological investigations have been conducted on the Dongping gold mineralization, but the results are extremely scattered, ranging from 350 Ma to 120 Ma (Table 5) and have led to contradictory interpretations of ore genesis (Hu and Luo, 1994; Jiang and Nie, 2000; Li et al., 1998, 2010; Wang, 1992; Xu et al., 2001). Most of the reported results were obtained using the Ar–Ar method on hydrothermal K-feldspar, quartz, and sericite (Hart et al., 2002; Jiang and Nie, 2000). The highly variable Ar–Ar results (290 Ma to ~153 Ma), which may suffer from either mixing of multistage hydrothermal minerals or gains/losses of Ar during multistage hydrothermal activities, cannot be related to any single tectonomagmatic event (Villa et al., 2013).

Zircon is commonly considered as an ideal dating method for geochronological studies because of its strong physical and chemical stability, as well as a closure temperature greater than 900 °C for the Th–U–

Table 2
LA-ICPMS U–Pb results for pristine zircons from the hornblende syenite*.

Spot no.	Th	U	Pb*	Th/U	$^{207}Pb/^{206}Pb$		$^{207}Pb/^{235}U$		$^{206}Pb/^{238}U$		$^{207}Pb/^{206}Pb$		$^{207}Pb/^{235}U$		$^{206}Pb/^{238}U$	
	ppm	ppm	ppm		Ratio	1σ	Ratio	1σ	Ratio	1σ	Age	1σ	Age	1σ	Age	1σ
D06-01.02	92.1	149	57.1	1.62	0.05627	0.00418	0.48867	0.03469	0.06298	0.00161	463	112	404	24	394	10
D06-01.03	94.9	147	42.4	1.55	0.05499	0.00464	0.48663	0.03933	0.06417	0.00181	412	130	403	27	401	11
D06-01.04	126	209	60.3	1.65	0.05275	0.00233	0.46989	0.01984	0.0646	0.00104	318	67	391	14	404	6
D06-01.05	35.8	93.3	25.2	2.61	0.05209	0.0038	0.45636	0.03212	0.06354	0.00144	289	119	382	22	397	9
D06-01.06	110	179	51.9	1.63	0.04707	0.00248	0.41819	0.02126	0.06443	0.00113	53	79	355	15	403	7
D06-01.07	37.0	77.8	26.3	2.10	0.05125	0.00519	0.47785	0.04681	0.06761	0.00202	252	166	397	32	422	12
D06-01.08	80.0	142	42.6	1.77	0.05521	0.00301	0.49045	0.02565	0.06442	0.00121	421	83	405	17	402	7
D06-01.09	85.1	165	45.9	1.93	0.05449	0.00299	0.47164	0.02476	0.06276	0.00122	391	83	392	17	392	7
D06-02.01	35.2	84.7	26.5	2.40	0.05584	0.00434	0.49294	0.03682	0.06403	0.00162	446	121	407	25	400	10
D06-02.02	64.6	112	28.3	1.74	0.05472	0.00473	0.48753	0.04063	0.06462	0.00173	401	139	403	28	404	10
D06-02.03	57.4	96.5	28.7	1.68	0.0551	0.00445	0.49719	0.03859	0.06545	0.00169	416	127	410	26	409	10
D06-02.04	49.9	112	31.3	2.24	0.05382	0.00412	0.47337	0.03478	0.06379	0.00159	364	121	394	24	399	10
D06-02.05	23.5	60.5	18.9	2.58	0.05476	0.00542	0.48897	0.04666	0.06476	0.00195	402	160	404	32	405	12
D06-02.06	33.6	81.6	24.1	2.43	0.05443	0.00402	0.48586	0.03452	0.06474	0.00155	389	117	402	24	404	9
D06-02.07	52.0	115	33.3	2.20	0.05549	0.00341	0.4883	0.0288	0.06382	0.00131	432	95	404	20	399	8
D06-02.08	20.9	48.7	13.9	2.32	0.05987	0.00615	0.52	0.05127	0.06299	0.00208	599	157	425	34	394	13
D06-02.09	35.7	102	28.0	2.86	0.05527	0.0047	0.48458	0.03952	0.06358	0.00177	423	133	401	27	397	11

* Represents radiogenic lead.

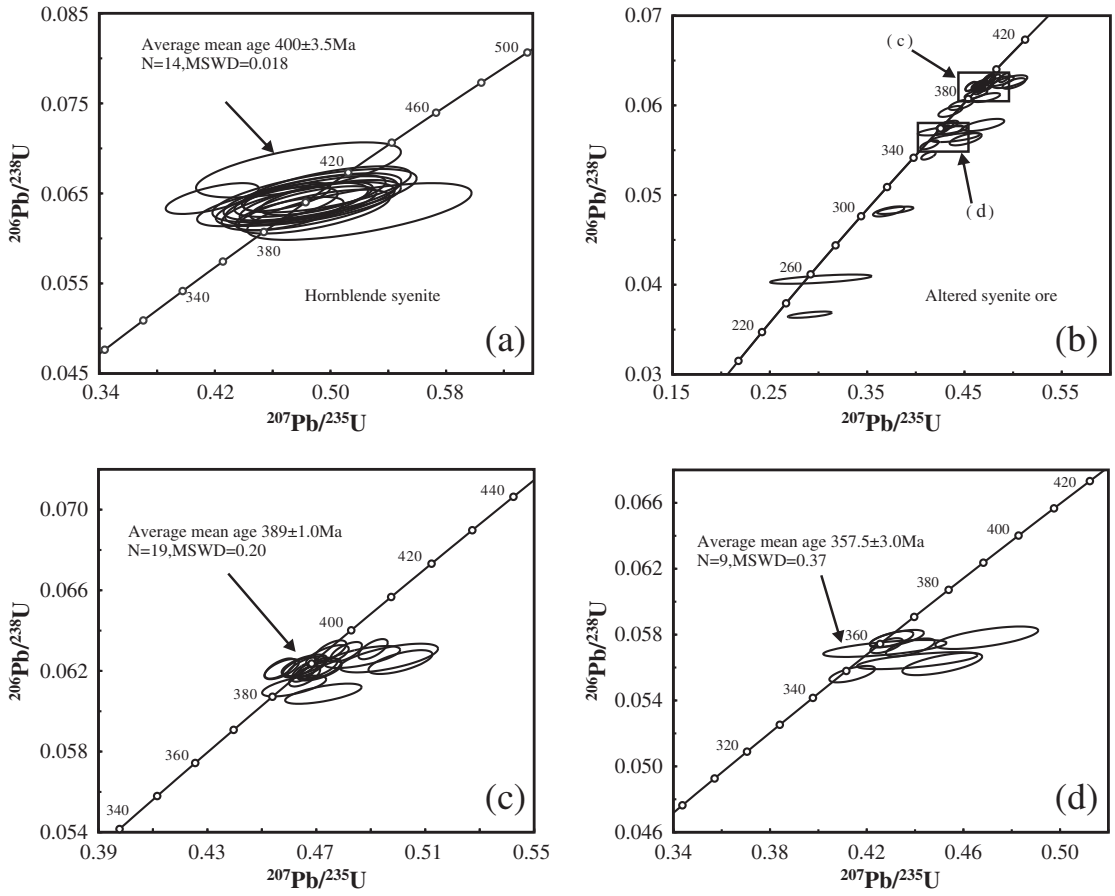

Fig. 7. U–Pb concordia plots for zircons from the hornblende syenite and disseminated ore.

Pb isotopic system (Lee et al., 1997). However, studies have shown that zircon may also crystallize at temperatures ranging from 600 to 300 °C, or even lower, from hydrothermal solutions or aqueous saturated relict melts (Geisler et al., 2003a,b,c; Martin-Martin et al., 2006; Pelleter et al., 2007; Rizvanova et al., 2000).

Some researchers have successfully dated mineralization using hydrothermal zircon from altered wall rocks and auriferous ores. Claoué Long et al. (1990) and Kerrich and King (1993) studied hydrothermal zircon from auriferous quartz veins from the Abitibi greenstone belt in Canada, and demonstrated that the zircon contained fluid inclusions and grains of native gold that formed at 260–380 °C and 200 MPa, and thus the U–Pb age of the zircon grains was interpreted to be the age of gold mineralization. Valley et al. (2009) dated an iron oxide copper–gold ore deposit using hydrothermal zircon grains separated from the ore that exhibit clear BSE images without internal structures. Hydrothermal zircon was also used to date exhumation of UHP eclogite (Wu et al., 2009).

Zircon grains from the hornblende syenite sampled in the northwestern corner of the Shuiquangou syenite complex are unambiguously magmatic and yield a LA–ICP-MS zircon U–Pb age of 400 ± 3.5 Ma, which represents the crystallization age of the syenite complex. The syenite along with other Devonian alkaline rocks and mafic–ultramafic complexes from neighboring regions occurring along the Shangyi–Chicheng deep fault constitute a linear post-collisional magmatic belt on the northern margin of the North China Craton, possibly formed under a tectonic regime of slab breakoff (Zhang and Zhai, 2010; Zhang et al., 2010a, b). During the Late Paleozoic to Mesozoic, the northern margin of the North China China Craton underwent several magmatic events (Zhang and Zhai, 2010). The hydrothermal processes in the Dongping area may be related to these multiphases of magmatic activities. Studies on fluid inclusions show that the Dongping gold deposit formed between 360 and 280 °C and 40 and 180 MPa (Mao et al., 2003), a condition favorable for hydrothermal zircon crystallization (Geisler et al., 2003a,b,c; Martin-Martin et al., 2006; Pelleter et al., 2007; Rizvanova et al., 2000). The zircon grains from the disseminated ore and from the gray auriferous quartz vein, which yield U–Pb ages of 389 ± 1.0 Ma and 385 ± 5.7 Ma, respectively, and exhibit CL images and U, Th, Pb, and REE concentrations, are different from those of the magmatic zircon. Therefore, the U–Pb dates of these hydrothermal zircon grains may identify an early stage of gold mineralization that is related to post-magmatic hydrothermal processes and pervasive metasomatism (Jiang et al., 2003).

The origin and geological significance of the eight analyses of zircon grains from the milky white auriferous quartz vein that have somewhat scattering U–Pb ages with a weighted mean age of 242 ± 6.8 Ma (Fig. 8c) are puzzling and open to debate. Three possible origins might be proposed for this group of zircon: they are 1) magmatic zircon derived from the neighboring intrusions and carried into the vein by hydrothermal fluids via fracture systems; 2) zircon precipitated from hydrothermal solutions related to the Triassic magmatism; and 3) hydrothermally altered magmatic zircon entrained from the syenite wall rock. However, none of the three hypotheses offer completely satisfactory explanations for the origin of the zircon grains, and thus the geological implication of the age is still unclear. Even though the U–Pb age of this group of zircon grains is roughly contemporaneous with the Triassic granite intrusions in the region (Jiang et al., 2007; Miao et al., 2002), the nearest granites occur more than 5 km away and make it improbable that the ~100 μm zircon grains were carried for such distances by fluid solutions through a fracture system. No geological field or microscopy evidence supports multiple stages of formation for the milky white quartz vein, so the zircon grains are unlikely to be of hydrothermal origin related to the Triassic granites in the neighboring area. The third

Table 3
LA-ICPMS U–Pb results for the zircons from the disseminated ore.

	Th	U	Pb	Th/U	$^{207}Pb/^{206}Pb$		$^{207}Pb/^{235}U$		$^{206}Pb/^{238}U$		$^{207}Pb/^{206}Pb$		$^{207}Pb/^{235}U$		$^{206}Pb/^{238}U$	
	ppm	ppm	ppm		Ratio	1σ	Ratio	1σ	Ratio	1σ	Age	1σ	Age	1σ	Age	1σ
BDP4A.01	17.0	144	39.7	0.12	0.05817	0.00104	0.50089	0.00775	0.06244	0.00039	536	23	412	5	390	2
BDP4A.03	56.2	281	61.6	0.20	0.07031	0.00156	0.47571	0.00952	0.04907	0.00037	453	67	321	8	303	2
BDP4A.04	5383	17563	3531	0.31	0.14939	0.00149	0.85634	0.00442	0.04157	0.00021	514	116	259	12	232	1
BDP4A.05	74.5	587	156	0.13	0.05583	0.00109	0.46371	0.00796	0.06023	0.0004	367	46	375	6	376	2
BDP4A.06	67.0	463	127	0.14	0.05487	0.00075	0.47021	0.00496	0.06214	0.00034	407	14	391	3	389	2
BDP4A.07	191	836	229	0.23	0.05510	0.00074	0.47181	0.00485	0.0621	0.00034	416	13	392	3	388	2
BDP4A.08	270	364	94.9	0.74	0.05325	0.00112	0.43560	0.00820	0.05932	0.0004	339	30	367	6	371	2
BDP4A.09	34.1	454	112	0.08	0.05613	0.00095	0.43156	0.00619	0.05575	0.00034	371	37	352	4	349	2
BDP4A.10	365	465	127	0.78	0.05440	0.00072	0.46661	0.00472	0.0622	0.00034	388	13	389	3	389	2
BDP4A.12	251	1265	345	0.20	0.05450	0.00059	0.46559	0.00311	0.06195	0.00032	392	7	388	2	387	2
BDP4A.13	235	1146	312	0.20	0.05470	0.00065	0.46568	0.00377	0.06173	0.00033	400	9	388	3	386	2
BDP4A.14	72.3	500	137	0.14	0.05340	0.00067	0.45725	0.00419	0.06209	0.00033	346	11	382	3	388	2
BDP4A.15	84.3	789	216	0.11	0.05330	0.00063	0.45664	0.00368	0.06212	0.00033	342	9	382	3	389	2
BDP4A.17	4794	11712	2864	0.41	0.11473	0.00114	0.82546	0.00430	0.05218	0.00026	487	75	326	9	304	2
BDP4A.19	41.2	202	54.1	0.20	0.07819	0.00169	0.63921	0.01243	0.05928	0.00045	564	69	391	10	362	3
BDP4A.20	947	4895	1208	0.19	0.06720	0.00074	0.51195	0.00354	0.05525	0.00029	415	30	351	4	341	2
BDP4A.21	40.4	298	81.8	0.14	0.05422	0.00080	0.46559	0.00550	0.06228	0.00035	380	17	388	4	389	2
BDP4A.22	72.5	797	218	0.09	0.05412	0.00068	0.46405	0.00423	0.06218	0.00033	376	11	387	3	389	2
BDP4A.24	100	947	241	0.11	0.05617	0.00071	0.44525	0.00415	0.05748	0.00031	378	27	362	3	359	2
BDP4A.26	88.8	300	77.3	0.30	0.05908	0.00091	0.47357	0.00602	0.05813	0.00034	383	42	365	5	362	2
BDP4A.27	71.6	469	120	0.15	0.05707	0.00084	0.45593	0.00543	0.05794	0.00033	374	34	363	4	362	2
BDP4A.28	54.1	370	92.2	0.15	0.05821	0.00152	0.45126	0.01090	0.05622	0.00045	538	39	378	8	353	3
BDP4A.29	119	727	184	0.16	0.05552	0.00098	0.43807	0.00667	0.05722	0.00036	433	23	369	5	359	2
BDP4B.02	573	2431	664	0.24	0.05583	0.00057	0.48492	0.00275	0.06298	0.00032	429	21	399	3	394	2
BDP4B.05	98.8	555	151	0.18	0.05469	0.00064	0.47519	0.00384	0.06300	0.00034	400	9	395	3	394	2
BDP4B.09	1498	3706	1035	0.40	0.07700	0.0008	0.66943	0.00393	0.06305	0.00033	400	41	386	5	383	2
BDP4B.11	2538	5233	1483	0.48	0.08657	0.00086	0.75607	0.00392	0.06333	0.00032	465	46	393	6	381	2
BDP4B.18	27.8	225	61.2	0.12	0.05478	0.00076	0.47409	0.00517	0.06275	0.00035	403	15	394	4	392	2
BDP4B.20	13.1	94	25.6	0.14	0.05899	0.00144	0.51057	0.01143	0.06276	0.00048	511	57	409	8	392	3
BDP4B.21	96.6	1078	298	0.09	0.06741	0.00076	0.58563	0.00429	0.063	0.00033	417	29	392	4	388	2
BDP4B.24	406	500	138	0.81	0.06242	0.00077	0.54389	0.00477	0.06318	0.00034	466	45	403	6	392	2
BDP4B.25	556	607	166	0.92	0.05643	0.00063	0.49082	0.00357	0.06308	0.00033	469	8	405	2	394	2
BDP4B.26	1410	4084	1183	0.35	0.12140	0.00124	1.04686	0.00597	0.06253	0.00032	382	92	361	12	358	2
BDP4B.28	1148	3791	1085	0.30	0.12305	0.00124	1.04672	0.00564	0.06168	0.00032	479	86	371	12	354	2
BDP4B.30	3073	6711	1830	0.46	0.23626	0.00234	1.7259	0.00876	0.05297	0.00027	372	261	268	27	257	2

possibility, that zircon entrained from the syenite wall rock experienced Pb-loss might be a more plausible interpretation. Zircon grains or domains can be altered by different processes, especially when metamict and followed by diffusion-reaction and/or fluid-driven dissolution–reprecipitation processes causing partial or total Pb-loss (e.g., Geisler et al., 2007; Gerdes and Zeh, 2009; Halpin et al., 2012; Mezger and Krogstad, 1997; Toscano et al., 2014). The rather low concentrations of actinides in the zircons (U 81–574 ppm, Th 215–1626 ppm), the short age interval (~150 Ma) between the time of original crystallization and proposed alteration, and the preserved magmatic zoning suggest little radiation damage. Even though solid volume diffusion has been demonstrated as a mechanism of Pb-loss in zircon, substantial diffusional Pb-loss from zircon is only possible at high temperatures (≥800 °C) and maintained for a few Ma (Ashwal et al., 1999; Bea and Montero,

Table 4
CAMECA ims-1280 SIMS U–Pb results for zircons from the auriferous quartz veins.

	U	Th	Th/U	f_{206}	$^{207}Pb/^{206}Pb$	±σ	$^{207}Pb/^{235}U$	±σ	$^{206}Pb/^{238}U$	±σ	$^{207}Pb/^{206}Pb$	±σ	$^{207}Pb/^{235}U$	±σ	$^{206}Pb/^{238}U$	±σ
	ppm	ppm		(%)		%		%		%						
Zircons from the milky white auriferous quartz vein																
D-19.1	536	354	0.66	0.03	0.05013	1.72	0.16698	2.31	0.0242	1.55	201.1	39.4	156.8	3.4	153.9	2.4
D-19.2	396	320	0.81	0.68	0.04821	3.35	0.15016	3.68	0.0226	1.52	109.5	77.2	142.0	4.9	144.0	2.2
D-19.19	1824	4566	2.50	1.03	0.04851	2.10	0.15577	2.64	0.0233	1.59	124.1	48.8	147.0	3.6	148.4	2.3
D-19.24	919	1480	1.61	0.28	0.04797	1.65	0.15033	2.23	0.0227	1.50	97.6	38.5	142.2	3.0	144.9	2.2
D-19.3	215	81	0.38	0.07	0.04999	2.53	0.27358	2.95	0.0397	1.51	194.7	57.7	245.6	6.4	250.9	3.7
D-19.20	1171	298	0.25	0.98	0.04969	1.11	0.24562	1.88	0.0358	1.51	180.6	25.8	223.0	3.8	227.1	3.4
D-19.21	282	185	0.65	0.05	0.05082	1.74	0.26657	2.30	0.0380	1.51	232.5	39.7	239.9	4.9	240.7	3.6
D-19.23	343	300	0.88	0.11	0.05016	1.70	0.27241	2.28	0.0394	1.52	202.6	39.0	244.6	5.0	249.0	3.7
D-19.25	303	171	0.56	0.00	0.05068	1.55	0.26647	2.16	0.0381	1.51	226.4	35.5	239.9	4.6	241.2	3.6
D-19.26	266	121	0.46	0.57	0.05104	3.73	0.26210	4.02	0.0372	1.50	242.8	83.8	236.4	8.5	235.7	3.5
D-19.27	570	127	0.22	2.37	0.05169	2.07	0.27517	2.56	0.0386	1.51	271.7	46.8	246.8	5.6	244.2	3.6
D-19.28	1626	574	0.35	0.02	0.05061	0.68	0.28225	1.78	0.0405	1.64	222.9	15.6	252.4	4.0	255.6	4.1
Zircons from the gray auriferous quartz vein																
D-77.8	54	4	0.08	0.26	0.05338	3.82	0.45272	4.11	0.0615	1.52	344.9	84.3	379.2	13.1	384.8	5.7
D-77.12	489	18	0.04	0.02	0.05439	1.03	0.46610	1.82	0.0622	1.50	387.1	23.1	388.5	5.9	388.7	5.7
D-77.16	185	29	0.16	0.03	0.05646	1.66	0.48185	2.24	0.0619	1.51	470.3	36.3	399.3	7.4	387.2	5.7
D-77.18	521	285	0.55	0.42	0.05503	1.42	0.46110	2.10	0.0608	1.55	413.5	31.5	385.0	6.8	380.3	5.7
D-77.10	68	61	0.89	0.46	0.15849	1.22	8.18256	2.00	0.3744	1.59	2439.6	20.5	2251.4	18.3	2050.3	28.0
D-77.11	26	124	4.76	0.00	0.11405	1.73	5.07985	2.30	0.3230	1.52	1864.9	30.9	1832.7	19.7	1804.6	23.9
D-77.17	56	50	0.89	0.02	0.14838	1.66	8.69832	2.25	0.4252	1.51	2327.3	28.2	2306.9	20.7	2283.9	29.1

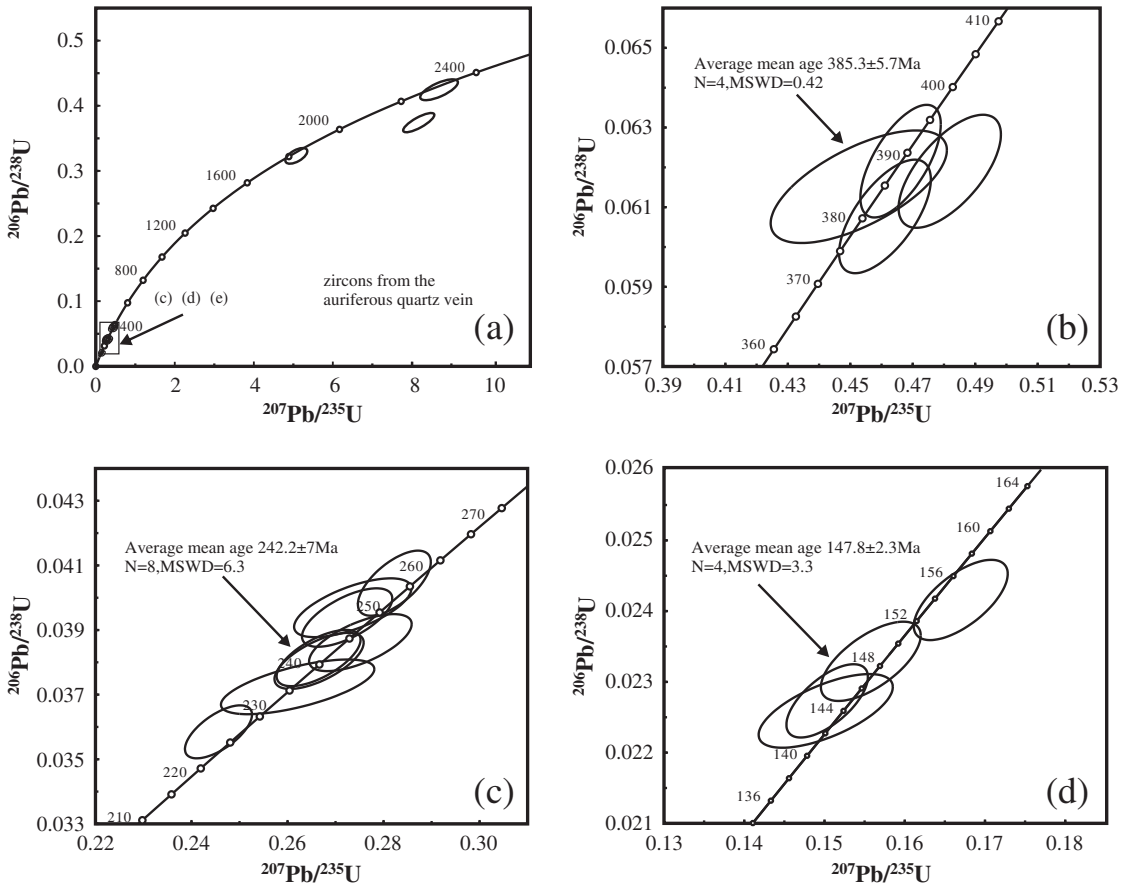

Fig. 8. U–Pb concordia plots for zircons from the auriferous quartz veins.

2013). As the Shuiquangou syenite complex has not experienced high grade metamorphism or high temperature thermal impacts after emplacement, Pb-loss through diffusiion is unlikely. Considering the occurrence of the zircon group with somewhat scattering U–Pb ages (~242 Ma), we argue that the zircon grains are possibly entrained from the syenites and/or metamorphic rocks rock and experienced Pb-loss through unrecognized mechanism during the hydrothermal processes.

The hydrothermal zircon grains from the low-grade milky white auriferous quartz vein in the Dongping gold deposit yield U–Pb ages of 147.8 ± 2.3 Ma, which may represent overprint effects of the Jurassic–Cretaceous Yanshanian hydrothermal event. This youngest stage of gold mineralization is roughly contemporary with intrusion of the Mesozoic Shangshuiquan syenogranite (142.5 ± 1.3 Ma, SHRIMP zircon U–Pb) and the Zhuanzhilian pyroxene diorite (139.5 ± 0.9 Ma, SHRIMP zircon U–Pb), which were emplaced adjacent to the syenite complex and the Donping mining area (Jiang et al., 2007; Miao et al., 2002). So, it can be deduced that this final stage of gold mineralization was related to the Yanshanian magmatism. A late Yanshanian gold event was also

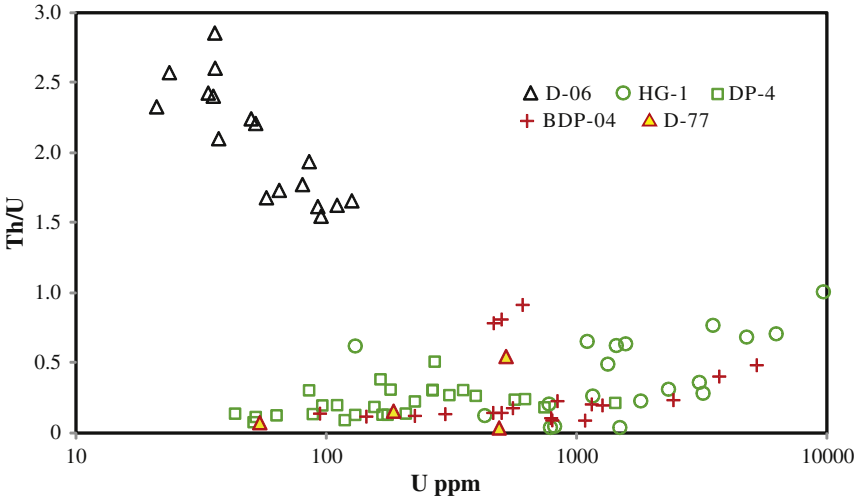

Fig. 9. U vs. Th/U diagram for the magmatic and hydrothermal zircons from the host rocks and ores (DP-4 and HG-1 are zircons from the Dongping and Hougou areas by Miao et al., 2002).

Table 5
Geochronological results from gold mineralization related to the Shuiquangou syenite complex.

Sampling location	Mineral or rock analyzed	Method	Age(Ma)	Source
Dongping gold deposit	Zircon, auriferous quartz vein	Conventional zircon U-Pb	350.9 ± 0.9	Li et al. (1998)
No.1 to N.70 vein group	Zircon, disseminated ore	LA–ICP-MS zircon U–Pb	389 ± 1	The authors
	K-feldspar, auriferous quartz vein	Ar–Ar	177.4 ± 5	Song and Zhao (1996)
	K-feldspar, auriferous quartz vein	Ar–Ar	156.7 ± 0.9	Lu et al. (1993)
	K-feldspar, disseminated ore	Ar–Ar	289.1 ± 0.3	Jiang et al. (2000)
	Sericite, disseminated ore	Ar–Ar	186.8 ± 0.3	Jiang and Nie (2000)
	Hydrothermal zircon, quartz vein	LA–ICP-MS zircon U–Pb	140.3 ± 1.4	Li et al. (2010)
	Zircon, low grade quartz vein	SIMS zircon U–Pb	242 ± 6.8	The author
	Zircon, low grade quartz vein	SIMS zircon U–P	147.8 ± 2.3	The author
	Muscovite, disseminated ore	Ar–Ar	153 ± 3	Hart et al. (2002)
	Fluid-inclusion, auriferous quartz vein	Rb–Sr isochron	103 ± 8	Mo et al. (1997)
Zhongshangou gold deposit	K-feldspar, auriferous altered rocks adjacent to quartz vein	Ar–Ar	241	Hart et al., 2002
Hougou gold deposit	Quartz, auriferous quartz vein	Ar–Ar	177.6 ± 1.9	Hu and Luo(1994)
	K-feldspar, auriferous quartz vein	Ar–Ar	172.9 ± 5	Wang, 1992
	K-feldspar, auriferous altered rock adjacent to quartz vein	Ar–Ar	288.1 ± 0.4	Jiang and Nie (2000)
	Sericite, auriferous altered rock adjacent to quartz vein	Ar–Ar	187.6 ± 0.4	Jiang and Nie (2000)
	K-feldspar, auriferous quartz vein	Laser probe Ar–Ar	202.6 ± 1.0	Xu et al. (2002)
Huangtuliang gold deposit	Sericite, auriferous altered rock adjacent to quartz vein	Ar–Ar	187.4 ± 0.3	Jiang and Nie (2000)

confirmed by LA–ICPMS zircon U–Pb dating of Li et al. (2010, 2012b) for the Dongping and Hougou area gold deposits, which yielded U–Pb ages of 141.2 ± 1.3 Ma and 154.4 ± 1.3, respectively.

5.2. Metallogenetic constraints placed by U–Pb ages of hydrothermal zircon

The Dongping gold deposit along with other adjacent gold deposits, including those at Zhongshangou, Jinjiazhuang, and Hougou, is spatially related to the Shuiquangou syenite complex, with all orebodies occurring inside of the complex or in the contact zones. Sulfur, Pb, Sr, and Si isotope compositions of the ore minerals and/or hydrothermal minerals related to the gold mineralization suggest that the ore metals were mainly derived from the syenite complex, although the Archaen metamorphic rocks may also have played a role (Bao and Zhao, 2006; Mo et al., 1997; Nie, 1998). Hydrogen-O isotope compositions of fluid inclusions show that the ore-forming fluids were predominantly magmatic solutions with some interaction by meteoric water (Bao and Zhao, 2006; Fan et al., 2001; Nie, 1998). Accordingly, the magmatism of the syenite complex was a principal factor controlling the formation of the gold deposit, and thus the gold deposits are akin to the genetic type of associated alkali rocks (Nie, 1998; Zhang et al., 2005).

The two groups of hydrothermal zircon grains from the disseminated ore and gray auriferous quartz vein, yielding roughly identical U–Pb ages of 389 ± 1.0 Ma and 385 ± 5.7 Ma, respectively, indicate that the ore deposit formed during the post-magmatic stage of syenite emplacement. Even though a group of zircon grains from the quartz vein yields a weighted mean age of 242 ± 6.8 Ma, which is similar to those of the Triassic granitic intrusions in the region, however, no geological evidence supports that there was a hydrothermal ore-forming processes associated with the Triassic magmatism. The ~140 Ma hydrothermal zircon from the auriferous quartz vein suggests Yanshanian hydrothermal superimposition. The predominance of post magmatic hydrothermal origin of the ore deposits confirms a genetic association with the Shuiquangou syenite as previously evidenced by S, Pb, and Si isotope compositions of the sulfide and quartz. Accordingly, it can now be accepted that the ore forming materials were mainly derived from the syenite complex.

6. Conclusions

1. LA–ICPMS zircon U–Pb dating of hornblende syenite from the western part of the Shuiquangou syenite complex yields a crystallization age of 400 ± 3.5 Ma (MSWD = 0.018). The previous zircon U–Pb ages for syenites from the Dongping mining area and the eastern part of the complex (390 ± 6 Ma and 386 ± 7 Ma, respectively) may represent the age of widespread pervasive post-magmatic hydrothermal alterations.
2. Hydrothermal zircon from the K-feldspathized–silicified syenite ore and auriferous quartz vein yield U–Pb ages of 389 ± 1.0 Ma and 385 ± 5.7 Ma, respectively, suggesting a post-magma origin for the main stage of gold mineralization in the Dongping gold deposit.
3. Hydrothermal zircon grains from the auriferous quartz vein yield a weighted mean U–Pb age of ~140 Ma, indicative of the overprinting of a late stage hydrothermal event.
4. The metallogenetic model of post-magmatic with late stage overprint for the gold mineralization well explains the close spatial and temporal association between the syenite complex and gold mineralization, as well as the pervasive K-feldspathization and silicification accompanying the gold mineralization.

Acknowledgments

This study is supported by the National Natural Science Foundation of China under Grant No.41372083 and No. 41121002. The authors thank the Dongping Gold Mine of the Zijin Mining Group, Dr. Cong-Ying Li at LA–ICPMS Laboratory of Guangzhou Institute of Geochemistry, and Qiu-li Li at Cameca Laboratory of Institute of Geology and Geophysics, Chinese Academy of Sciences for their kind cooperation and assistance during field investigation and laboratory analysis. We thank Prof. R.J. Goldfarb for his constructive comments and suggestions. Many thanks to Prof. Robert E. Zartman for his intensive editing and helpful comments.

References

Andersen, T., 2002. Correction of common lead in U–Pb analyses that do not report ^{204}Pb. Chem. Geol. 192, 59–79.
Ashwal, L.D., Tucker, R.D., Zinner, E.K., 1999. Slow cooling of deep crustal granulites and Pb-loss in zircon. Geochim. Cosmochim. Acta 63, 2839–2851.
Bao, Z.W., Zhao, Z.H., 2006. Isotopic geochemical constrains on metallogeny of the Dongping-type gold deposits associated with syenites. Acta Petrol. Sin. 22, 2534–2542 (In Chinese with English abstract).
Bao, Z.W., Zhao, Z.H., Zhang, P.H., Wang, Y.X., 2003. REE, Sr, Nd, and Pb isotopic evidence for the petrogenesis of the Shuiquangou syenite complex in NW Hebei province. China. Geol. Rev. 49, 621–627 (In Chinese with English abstract).
Bea, F., Montero, P., 2013. Diffusion-induced disturbances of the U–Pb isotope system in pre-magmatic zircon and their influence on SIMS dating. A numerical study. Chem. Geol. 349–350, 1–17.
Berger, G.W., 1975. ^{40}Ar/^{39}Ar step heating of thermally overprinted biotite, hornblende and potassium feldspar from Eldora, Colorado. Earth Planet. Sci. Lett. 26, 387–408.
Black, L.P., Kamo, S.L., Allen, C.M., Aleinikoff, J.N., Davis, D.W., Korsch, R.J., Foudoulis, C., 2003. TEMORA 1: a new zircon standard for Phanerozoic U–Pb geochronology. Chem. Geol. 200, 155–170.
Boynton, W.V., 1984. Cosmochemistry of the rare earth elements: meteorite studies. In: Henderson, P. (Ed.), Rare Earth Element Geochemistry. Elsevier, Amsterdam, pp. 63–114.
Chen, Y.X., Zheng, Y.F., Chen, R.X., Zhang, S.B., Li, Q.L., Dai, M.N., Chen, L., 2011. Metamorphic growth and recrystallization of zircons in extremely ^{18}O-depleted rocks during eclogite-facies metamorphism: evidence from U–Pb ages, trace elements, and O–Hf isotopes. Geochim. Cosmochim. Acta 75, 4877–4898.

Claoué Long, J.C., King, R.W., Kerrich, R., 1990. Archaean hydrothermal zircon in the Abitibi greenstone belt: constraints on the timing of gold mineralisation. Earth Planet. Sci. Lett. 98, 109–128.
Cook, N.J., Ciobanu, C.L., Mao, J.W., 2009. Textural control on gold distribution in As-free pyrite from the Dongping, Huangtuliang and Hougou gold deposits, North China Craton (Hebei Province, China). Chem. Geol. 264, 101–121.
Deng, J.F., Su, S.G., Niu, Y.L., Liu, C., Zhao, G.C., Zhao, X.G., Zhou, S., Wu, Z.X., 2007. A possible model for the lithospheric thinning of North China Craton: evidence from the Yanshanian (Jura-Cretaceous) magmatism and tectonism. Lithos 96, 22–35.
Fan, H.R., Xie, Y.H., Zhai, M.G., 2001. Ore-forming fluids in the Dongping gold deposit, northwestern Hebei Province. Sci. China (D) 44, 748–757.
Gao, S., Rudnick, R.L., Carlson, R.W., McDonough, W.F., Liu, Y.S., 2002. Re–Os evidence for replacement of ancient mantle lithosphere beneath the North China craton. Earth Planet. Sci. Lett. 198, 307–322.
Geisler, T., Pidgeon, R.T., Kurtz, R., van Bronswijk, W., Schleicher, H., 2003a. Experimental hydrothermal alteration of partially metamict zircon. Am. Mineral. 88, 1496–1513.
Geisler, T., Zhang, M., Salje, E.K.H., 2003b. Recrystallization of almost fully amorphous zircon under hydrothermal conditions: an infrared spectroscopic study. J. Nucl. Mater. 320, 280–291.
Geisler, T., Rashwan, A.A., Rahn, M.K.W., Poller, U., Zwingmann, H., Pidgeon, R.T., Schleicher, H., Tomaschek, F., 2003c. Low-temperature hydrothermal alteration of natural metamict zircons from the eastern desert, Egypt. Mineral. Mag. 67, 485–508.
Geisler, T., Schaltegger, U., Tomaschek, F., 2007. Re-equilibration of zircon in aqueous fluids and melts. Elements 3, 43–50.
Gerdes, A., Zeh, A., 2009. Zircon formation versus zircon alteration — New insights from combined U–Pb and Lu–Hf in-situ LA–ICP-MS analyses, and consequences for the interpretation of Archean zircon from the Central Zone of the Limpopo Belt. Chem. Geol. 261, 230–243.
Goldfarb, R.J., Groves, D.I., Gardoll, S., 2001. Orogenic gold and geologic time: a global synthesis. Ore Geol. Rev. 18, 1–75.
Halpin, J.A., Daczko, N.R., Milan, L.A., Clarke, G.L., 2012. Decoding near-concordant U–Pb zircon ages spanning several hundred million years: recrystallisation, metamictisation or diffusion? Contrib. Mineral. Petrol. 163, 67–85.
Hart, C.J.R., Goldfarb, R.J., Qiu, Y.M., Snee, L., Miller, L.D., Miller, M.L., 2002. Gold deposits of the northern margin of the North China Craton: multiple late Paleozoic–Mesozoic mineralizing events. Miner. Deposita 37, 326–351.
Hoskin, P.W.O., 2005. Trace-element composition of hydrothermal zircon and the alteration of Hadean zircon from the Jack Hills, Australia. Geochim. Cosmochim. Acta 69, 637–648.
Hoskin, P., Schaltegger, U., 2003. The composition of zircon and igneous and metamorphic petrogenesis. In: Hanchar, J., Hoskin, P. (Eds.), Zircon. Rev. Mineral. Geochem, 53, pp. 27–62.
Hu, D.X., Luo, G.L., 1994. $^{40}Ar/^{39}Ar$ ages of gold-bearing quartz veins and their geological significance in typical gold deposits of Zhangjiakou–Xuanhua gold field, Hebei province. Sci. Geol. Sin. 29, 151–158 (In Chinese with English abstract).
Hu, L., Song, H.L., 2002. Age of activities of the southern "Inner Mongolian axis" marginal fault belt and an analysis of its structure. Chin. Geol. 29, 369–373 (In Chinese with English abstract).
Hu, L., Song, H.L., Yan, D.P., Hu, D.G., 2003. The $^{40}Ar/^{39}Ar$ geochronology constraint and geological significance of mylonites in Shangyi–Chicheng fault belt on the north of North China Craton. Sci. China (D) 46, 1134–1141.
Jiang, N., 2005. Petrology and geochemistry of the Shuiquangou syenitic complex, northern margin of the North China Craton. J. Geol. Soc. Lond. 162, 203–215.
Jiang, N., 2006. Hydrothermal alteration of chevkinite-(Ce) in the Shuiquangou syenitic intrusion, northern China. Chem. Geol. 227, 100–112.
Jiang, S.H., Nie, F.J., 2000. $^{40}Ar–^{39}Ar$ geochronology of the Shuiquangou alkaline complex and related gold deposits, Northwestern Hebei, China. Geol. Rev. 46, 621–627 (In Chinese with English abstract).
Jiang, N., Sun, S.H., Chu, X.L., Mizutab, T., Ishiyama, D., 2003. Mobilization and enrichment of high-field strength elements during late and post-magmatic processes in the Shuiquangou syenitic complex, Northern China. Chem. Geol. 200, 117–128.
Jiang, N., Liu, Y.S., Zhou, W.G., Yang, J.H., Zhang, S.Q., 2007. Derivation of Mesozoic adakitic magmas from ancient lower crust in the North China craton. Geochim. Cosmochim. Acta 71, 2591–2608.
Kerrich, R., King, R., 1993. Hydrothermal zircon and baddeleyite in Vald'Or Archean mesothermal gold deposits: characteristics, compositions and fluid-inclusion properties, with implications for timing of primary gold mineralization. Can. J. Earth Sci. 30, 2334–2351.
Kirkland, C.L., Whitehouse, M.J., Slagstad, T., 2009. Fluid-assisted zircon and monazite growth within a shear zone: a case study from Finnmark, Arctic Norway. Contrib. Mineral. Petrol. 158, 637–657.
Kuiper, Y.D., 2002. The interpretation of inverse isochron diagrams in $^{40}Ar/^{39}Ar$ geochronology. Earth Planet. Sci. Lett. 203, 499–506.
Lawrie, K.C., Memagh, T.P., Ryan, C.G., van Achterbergh, E., Blacket, L.P., 2007. Chemical fingerprinting of hydrothermal zircons: an example from the Gidginbung high sulphidation Au–Ag–(Cu) deposit, New South Wales, Australia. Proc. Geol. Assoc. 118, 37–46.
Lee, J.K.W., Willians, I.S., Ellis, D.J., 1997. Pb, U and Th diffusion in natural zircon. Nature 390, 159–161.
Li, C.J., Bao, Z.W., 2012. Geochemical characteristics and geodynamic implications of the Early Cretaceous magmatism in Zhangjiakou area, northwest Hebei province. Geochimica 41, 343–358 (In Chinese with English abstract).
Li, H.M., Li, H.K., Lu, S.N., Yang, C.L., 1998. Determination of age of gold mineralization of Dongping gold deposits by U–Pb dating hydrothermal zircons from ore veins. (sup) Acta Geosci. Sin. 18, 176–178 (In Chinese).
Li, X.H., Liu, Y., Li, Q.L., Guo, C.H., Chamberlain, K.R., 2009. Precise determination of Phanerozoic zircon Pb/Pb age by multi-collector SIMS without external standardization. Geochem. Geophys. Geosyst. 10. http://dx.doi.org/10.1029/2009GC00 2400 (Q04010).
Li, C.M., Deng, J.F., Chen, L.H., Su, S.G., Li, H.M., Hu, S.L., 2010. Two periods of zircon from Dongping gold deposit in Zhangjiakou–Xuanhua area, northern margin of North China: constraints on metallogenic chronology. Miner. Depos. 29, 265–275 (In Chinese with English abstract).
Li, C.Y., Zhang, H., Wang, F.Y., Liu, J.Q., Sun, Y.L., Hao, X.L., Li, Y.L., Sun, W.D., 2012a. The formation of the Dabaoshan porphyry molybdenum deposit induced by slab rollback. Lithos 150, 101–110.
Li, C.M., Li, T., Deng, J.F., Su, S.G., Liu, X.M., 2012b. LA–ICP-MS zircon U–Pb age of the brittle-ductile shear zones in Hougou gold deposit, Northwestern Hebei Province. Geotecton. Metallog. 36, 157–167 (In Chinese with English abstract).
Li, S.R., Santosh, M., Zhang, H.F., Shen, J.F., Dong, G.C., Wang, J.Z., Zhang, J.Q., 2013. Inhomogeneous lithospheric thinning in the central North China Craton: zircon U–Pb and S–He–Ar isotopic record from magmatism and metallogeny in the Taihang Mountains. Gondwana Res. 23, 141–160.
Liang, J.L., Ding, X., Sun, X.M., Zhang, Z.M., Zhang, H., Sun, W.D., 2009. Nb/Ta fractionation observed in eclogites from the Chinese Continental Scientific Drilling Project. Chem. Geol. 268, 27–40.
Liu, Y., Gao, S., Hu, Z., Gao, C., Zong, K., Wang, D., 2010. Continental and oceanic crust recycling-induced melt–peridotite interactions in the trans-north China Orogen: U–Pb dating, Hf isotopes and trace elements in Zircons from Mantle Xenoliths. J. Petrol. 51, 537–571.
Liu, S.A., Li, S.G., Guo, S.S., Hou, Z.H., He, Y.S., 2012. The Cretaceous adakitic–basaltic–granitic magma sequence on south-eastern margin of the North China Craton: implications for lithospheric thinning mechanism. Lithos 134–135, 163–178.
Lu, D.L., Wang, J.J., Luo, X.Q., Zhang, S.H., Zheng, B.Y., 1993. The metallogenic epoch of the Dongping gold deposit. Miner. Depos. 12, 182–188 (In Chinese with English abstract).
Lu, S.N., Li, H.K., Li, H.M., Yang, C.L., Hu, Z.D., Jiang, M.M., 1997. The characteristics of basements and metallogenetic study of gold deposit concentrated areas. Geol. Publ. house 6–44 (In Chinese).
Ludwig, K.R., 2001. Users manual for Isoplot/Ex rev. 2.49. Berkeley Geochronol. Cent. Spec. Publ. v. 1a, 1–56.
Ludwig, K.R., 2003. ISOPLOT 3.0: a geochronological toolkit for Microsoft excel. Berkeley Geochronol. Cent. Spec. Publ. *No. 4*, 1–71.
Ma, Z.J., Zhao, J.M., 1999. Contrast research on Tianshan orogenic belt and Yinshan–Yanshan orogenic belt. Earth Sci. Front. 6, 95–102 (In Chinese with English abstract).
Mao, J.W., Li, Y.Q., 2001. Fluid inclusions of the Dongping gold telluride deposit in Hebei Province, China: involvement of mantle fluid in metallogenesis. Miner. Depos. 20, 23–36 (In Chinese with English abstract).
Mao, J.W., Li, Y.Q., Goldfarb, R.J., He, Y., Zaw, K., 2003. Fluid inclusion and noble gas studies of the Dongping gold deposit, Hebei Province, China: a mantle connection for mineralization? Econ. Geol. 98, 517–534.
Martin-Martin, J.D., Tritlla, J., Cardellach, E., Gómez-Gras, D., 2006. Tectonically driven fluid flow and associated low-grade metamorphism during the Alpine compression in the eastern Iberian Chain (Spain). J. Geochem. Explor. 89, 267–270.
Menzies, M., Xu, Y.G., Zhang, H.F., Fan, W.M., 2007. Integration of geology, geophysics and geochemistry: a key to understanding the North China Craton. Lithos 96, 1–21.
Mezger, K., Krogstad, E.J., 1997. Interpretation of discordant U–Pb zircon ages: an evaluation. J. Metamorph. Geol. 15, 127–140.
Miao, L.C., Qiu, Y.M., McNaughton, N., Luo, Z.K., Groves, D., Zhai, Y.S., Fan, W.M., Zhai, M.G., Guan, K., 2002. SHRIMP U–Pb zircon geochronology of granitoids from Dongping area, Hebei Province, China: constraints on tectonic evolution and geodynamic setting for gold metallogeny. Ore Geol. Rev. 19, 187–204.
Mo, C.H., 1996. Geochemistry and metallogeny of gold deposits in Zhangjiakou area. [Doctorate thesis]. Guangzhou: Guangzhou Institute of Geochemistry. Chin. Acad. Sci. 1–48 (In Chinese with English abstract).
Mo, C.H., Wang, X.Z., Cheng, J.P., Liang, H.Y., 1997. Rb–Sr isochron determination for fluid inclusions within quartz vein from Dongping gold deposit, NW Hebei province and its implications for metallogeny. Geochimica 16, 20–27 (In Chinese with English abstract).
Nie, F.J., 1998. Geology and origin of the Dongping alkali-type gold deposit, Northern Hebei Province, People's Republic of China. Resour. Geol. 48, 139–158.
Nie, F.J., Jiang, S.H., Liu, Y., 2004. Intrusion-related gold deposits of North China Craton, People's Republic of China. Resour. Geol. 54, 299–324.
Pelleter, E., Cheilletz, A., Gasquet, D., Mouttaqi, A., Annich, M. El, Hakour, A., Deloule, E., Feraud, G., 2007. Hydrothermal zircons: a tool for ion microprobe U–Pb dating of gold mineralization (Tamlalt–Menhouhou gold deposit Morocco). Chem. Geol. 245, 135–161.
Pettke, T., Audétat, A., Schaltegger, U., Heinrich, C.A., 2005. Magmatic-to-hydrothermal crystallization in the W–Sn mineralized Mole Granite (NSW, Australia) part II: evolving zircon and thorite trace element chemistry. Chem. Geol. 220, 191–213.
Rizvanova, N.G., Levchenkov, O.A., Belous, A.E., Bezmen, N.I., Maslenikov, A.V., Komarov, A.N., Makeev, A.F., Levskiyet, L.K., 2000. Zircon reaction and stability of the U–Pb isotope system during interaction with carbonate fluid: experimental hydrothermal study. Contrib. Mineral. Petrol. 139, 101–114.
Song, G.R., Zhao, Z.H., 1996. Geology of Dongping Alkaline Complex-Hosted Gold Deposit in Hebei Province. Seismological Press, Beijing, pp. 1–170 (In Chinese with English abstract).
Sun, W.D., Li, S., Yang, X.Y., Ling, M.X., Ding, X., Duan, L.A., Zhan, M.Z., Zhang, H., Fan, W.M., 2013. Large-scale gold mineralization in eastern China induced by an Early Cretaceous clockwise change in Pacific plate motions. Int. Geol. Rev. 55, 311–321.

Toscano, M., Pascual, E., Nesbitt, R.W., Almodóvar, G.R., Sáez, R., Donaire, T., 2014. Geochemical discrimination of hydrothermal and igneous zircon in the Iberian Pyrite Belt, Spain. Ore Geol. Rev. 56, 301–311.

Valley, P.M., Hanchar, J.M., Whitehouse, M.J., 2009. Direct dating of Fe oxide-(Cu–Au) mineralization by U/Pb zircon geochronology. Geology 37, 223–226.

Villa, I.M., Williams, M.L., 2013. Geochronology of metasomatic events. In: Harlov, D.E., Austrheim, H. (Eds.), Metasomatism and the Chemical Transformation of Rock, Lecture Notes in Earth System Sciences. Springer-Verlag, Berlin Heidelberg, pp. 171–202.

Wang, R.R., 1992. The characteristics and genesis of the felsic alkali complex, Jinjiazhuang, Hebei. J. Guilin Inst. Technol. 12, 12–20 (In Chinese with English abstract).

Wilde, S.A., Zhou, X.H., Nemchin, A.A., Sun, M., 2003. Mesozoic crust–mantle interaction beneath the North China craton: a consequence of the dispersal of Gondwanaland and accretion of Asia. Geology 31, 817–820.

Wu, Y.B., Zheng, Y.F., 2004. Genesis of zircon and its constraints on interpretation of U–Pb age. Chin. Sci. Bull. 49, 1554–1569.

Wu, Y.B., Gao, S., Zhang, H.F., Yang, S.H., Liu, X.C., Jiao, W.F., Liu, Y.S., Yuan, H.L., Gong, H.J., He, M.C., 2009. U–Pb age, trace-element, and Hf-isotope compositions of zircon in a quartz vein from eclogite in the western Dabie Mountains: constraints on fluid flow during early exhumation of ultrahigh-pressure rocks. Am. Mineral. 94, 303–312.

Xu, X.W., Cai, X.P., Liu, Y.L., Zhang, B.L., 2002. Laser probe ^{40}Ar–^{39}Ar ages of metasomatic K-feldspar from the Hougou gold deposit, northwestern Hebei Province China. Sci. China (D) 45, 559–564.

Xu, W.L., Zhou, Q.J., Pei, F.P., Yang, D.B., Gao, S., Li, Q.L., Yan, Y.H., 2013. Destruction of the North China Craton: delamination or thermal/chemical erosion? Mineral chemistry and oxygen isotope insights from websterite xenoliths. Gondwana Res. 23, 119–129.

Yang, W.B., Niu, H., Sun, W.D., Shan, Q., Zheng, Y.F., Li, N.B., Li, C.Y., Arndt, N.T., Xu, X., Jiang, Y.H., Yu, X.Y., 2013. Isotopic evidence for continental ice sheet in mid-latitude region in the supergreenhouse Early Cretaceous. Sci. Rep. 3. http://dx.doi.org/10.1038/srep02732.

Yuan, H.L., Gao, S., Liu, X.M., Li, H.M., Günther, D., Wu, F.Y., 2004. Accurate U–Pb age and trace element determinations of zircon by laser ablation-inductively coupled plasma mass spectrometry. Geostand. Geoanal. Res. 28, 353–370.

Zartman, R.E., Smith, J.V., 2009. Mineralogy and U–Th–Pb ages of a uranium-bearing jasperoid vein from the Sunshine mine, Coeur d'Alene district, Idaho. Chem. Geol. 261, 184–194.

Zhang, Z.C., 1996. Characteristics of H and O isotopes and fluid evolution in Dongping gold deposit. Gold Geol. 2, 36–41 (In Chinese with English abstract).

Zhang, X.H., Zhai, M.G., 2010. Magmatism and its metallogenetic effects during the Paleozoic continental crustal construction in northern North China: an overview. Acta Petrol. Sin. 26, 1329–1341 (In Chinese with English abstract).

Zhang, P.H., Zhao, Z.H., Bao, Z.W., Wang, Y.X., Li, S.Z., Zhang, Y.H., 2001. The distribution pattern of gold and tellurium and their correlation of ores from the Dongping gold mine. Geol. Prospect. 37 (3), 24–28 (in Chinese with English abstract).

Zhang, J.H., Jiang, S.H., Nie, F.J., 2005. Geological features of the Hougou and Huangtuliang gold deposits, northwestern Hebei Province. In: Jiang, S.H., Zhang, J.H., Nie, F.J. (Eds.), Field Trip Guide No. 7, Intrusion-Related Gold Deposits of the Northern Margin of the North China Craton, Hebei Province, China, 8th Biennial SGA Meeting, 18–21 August 2005, Beijing, China. 12.

Zhang, S.H., Zhao, Y., Liu, J., Hu, J.M., Chen, Z.L., Pei, J.L., Chen, Z.Y., Zhou, J.X., 2007. Emplacement depths of the Late Paleozoic–Mesozoic grantoid intrusions from the northern North China block and their tectonic implications. Acta Petrol. Sin. 23, 625–638 (In Chinese with English abstract).

Zhang, S.H., Zhao, Y., Liu, J., Hu, J.M., Song, B., Liu, J., Wu, H., 2010a. Geochronology, geochemistry and tectonic setting of the Late Paleozoic–Early Mesozoic magmatism in the northern margin of the North China Block: a preliminary review. Acta Petrol. Mineral. 29, 824–842 (In Chinese with English abstract).

Zhang, X.H., Zhang, H.F., Jiang, N., Zhai, M.G., Zhang, Y.B., 2010b. Early Devonian alkaline intrusive complex from the northern North China craton: a petrological monitor of post-collisional tectonics. J. Geol. Soc. (Lond.) 167, 717–730.

Zhao, Z.H., Bao, Z.W., Qiao, Y.L., 2010. A peculiar composite M- and W-type REE tetrad effect: evidence from the Shuiquangou alkaline syenite complex, Hebei Province, China. Chin. Sci. Bull. 55, 2684–2696.

Zhu, R.X., Xu, Y.G., Zhu, G., Zhang, H.F., Xia, Q.K., Zheng, T.Y., 2012. Destruction of the North China Craton. Sci. China (D) 55, 1565–1587.